nature research

https://doi.org/10.1038/s41929-020-00557-y

Supplementary information

A new-to-nature carboxylation module to improve natural and synthetic CO_2 fixation

In the format provided by the authors and unedited

Supplementary Information

A new-to-nature carboxylation module to improve natural and synthetic CO_2 fixation

Marieke Scheffen, Daniel G. Marchal, Thomas Beneyton, Sandra K. Schuller, Melanie Klose, Christoph Diehl, Jessica Lehmann, Pascal Pfister, Martina Carrillo, Hai He, Selçuk Aslan, Niña S. Cortina, Peter Claus, Daniel Bollschweiler, Jean-Christophe Baret, Jan M. Schuller, Jan Zarzycki, Arren Bar-Even, Tobias J. Erb*

*Correspondence to: toerb@mpi-marburg.mpg.de

This PDF file includes

Supplementary Methods

Synthesis of CoA esters. Glycolyl-CoA was synthesized as previously described[1]. Tartronyl-CoA was enzymatically synthesized using the malonyl-CoA synthetase MatB[2]. The preparation contained in a total volume of 10 mL 200 mM MOPS/KOH pH 7.8, 20 mM tartronate, 7.5 mM ATP, 10 mM $MgCl_2$, 5 mM coenzyme A and 600 µg MatB. The reaction was performed for 18.5 h at room temperature, quenched with 1% HCl and centrifuged at 17.000 × *g* for 20 min. CoA esters were purified using preparative HPLC. The synthesis mixtures were applied to a preparative Agilent 1260 Infinity HPLC with a Gemini 10 µm NX-C18 110 Å column (Phenomenex). Chromatographic separation was achieved using 25 mM ammonium formate pH 4.2 with a methanol gradient from 1% to 30% at a flow rate of 25 mL min^{-1}. Glycolyl-CoA or tartronyl-CoA fractions, respectively, were pooled, flash-frozen in liquid nitrogen, and lyophilized. The concentration of CoA-esters was quantified by determining the absorption at 260 nm (ε=16.4 mM^{-1} cm^{-1}).

Cloning of expression vectors. All *in silico* cloning was performed with Clone Manager 9 (Scientific & Educational Software). For purification, preparation, cloning, transformation and amplification of DNA, standard protocols were used[3]. Plasmid isolation and PCR-product purification was performed according to the manufacturer's protocols using the kits NucleoSpin® Plasmid (Macherey Nagel) and NucleoSpin® Gel and PCR Clean-up (Macherey Nagel). All primers used in this study were synthesized by Eurofins Genomics Germany GmbH. All primers used in this study can be found in Supplementary Table 6 and all plasmids are listed in Supplementary Table 7. The plasmids of propionate CoA transferase from *Clostridium propionicum* (pET-16b_PCT) and *Ralstonia eutropha* (pET-19b::pct) were kind gifts from I. Berg, Münster (Germany) and A. Steinbüchel, Münster (Germany), respectively. The plasmid of the water-forming NADH oxidase from *Lactobacillus pentosus* (pET28a-NH-nox-L.p.) was a kind gift from V. Sieber, Straubing (Germany). The plasmid for the AMP-regenerating polyphosphate kinase (pET28a-AjPKK2) was a kind gift from J. Andexer, Freiburg (Germany). For the construction of the expression plasmid for 4-OH-butyrate CoA transferase (AbfT) from *Clostridium aminobutyricum* (pTE1138), the gene was ordered codon-optimized and cloned into a pET16b derivative using XbaI and KpnI for restriction. The genes encoding for *Ery*ACS1 and *Ery*ACS2 were synthesized codon-optimized for *E. coli* and cloned into the backbone pSEVA141 by the DOE Joint Genome Institute (JGI) (ACS1, pTE1007) or pSEVA261 (ACS2, pTE1008), respectively. For the construction of the expression vectors for the ACS1 mutants ACS1_V379G (pTE1434), ACS1_V379S (pTE1418), ACS1_V379A

(pTE1417) and ACS1_V379A_L641P (pTE1427), single-oligo directed mutagenesis was performed[4] using the primers ACS_Ery_V379G, ACS_Ery_V379S, ACS_Ery_V379A and ACS_Ery_L641P, respectively. The gene encoding for the ligase domain of the propionyl-CoA synthase (*Ery*PCS_lig) was synthesized by the JGI and subcloned into the vector pET16b, using NdeI and BamHI restriction sites, resulting in plasmid pJZ26. The genes encoding for the two subunits of propionyl-CoA carboxylases from *Chloroflexus aurantiacus* (*Ca*PCC1 and *Ca*PCC2) were synthesized by the JGI and subcloned as dicistrons into the vector pT7-7[5], using NdeI and BamHI restriction sites, resulting in plasmids pJZ95 and pJZ96. The genes encoding for the two subunits of propionyl-CoA carboxylases from *Erythrobacter sp.* NAP1 (*Ery*PCC) were synthesized by the JGI and subcloned into the vector pCDFDuet-1 (Novagen, Merck), using NcoI/HindIII and NdeI/XhoI restriction sites, resulting in plasmid pJZ151. For the expression of PCC from *Methylorubrum extorquens* AM1, plasmid pTE615 was used[6]. The PCC plasmids containing the PCC mutants PCC_LD (pJZ99), PCC_LN (pJZ100), PCC_YE (pJZ101), PCC_YH (pJZ141), PCC_YQ (pJZ102), PCC_GA (pJZ127), PCC_GS (pJZ117), PCC_GT (pJZ118), PCC_DI (pJZ105) and PCC_DK (pJZ103), were obtained by performing single-oligo directed mutagenesis[4] using the primers PCCtoGCC_L140D, PCCtoGCC_L140N, PCCtoGCC_Y143E, PCC_Y143H, PCCtoGCC_Y143Q, PCC_G170A, PCC_G170S, PCC_G170T, PCCtoACC_D407I and PCCtoGCC_D407K, respectively, using pTE615 as a template (Supplementary Table 8). The plasmid for GCC M2 (pJZ133) was obtained by performing single-oligo mutagenesis[4] on pJZ105 using the primer PCC_Y143H. The plasmids containing GCC_M2_LD (pTE1411), GCC_M2_LN (pTE1413) and GCC M3 (pTE1412) were created by single-oligo mutagenesis[4] using pJZ133 as a template and PCC_L100D, PCC_L100N, PCC_L100S as primers, respectively (Supplementary Table 7). The plasmids pTE1422 and pTE1425 were created by performing single-oligo mutagenesis[4] on pTE1412 using the primers PCCMe_D171A and PCCMe_D171V, respectively (Supplementary Table 6, Supplementary Table 7). The plasmid for GCC M4 was obtained from isolation after screening the random mutagenesis library of pTE1412 and was termed pTE3100. The plasmid for GCC M5 was obtained from isolation after screening the random mutagenesis library of pTE3100 and was termed pTE3101. The gene of malonyl-CoA reductase from *Erythrobacter* sp. NAP1 was synthesized codon-optimized for *E. coli* by JGI and obtained subcloned into pSEVA 321 (pTE1010). The *birA* gene from *M. extorquens* AM1 was amplified from isolated genomic DNA, via flanking primers including restrictions sites for NdeI (BirA_Me_bb_for) and BamHI (BirA_Me_bb_rev, Supplementary Table 6). The PCR product was inserted into the expression vector pET16b via restriction digestion by the respective

enzymes and ligation. Single-oligo directed mutagenesis[4] was used to remove an EcoRI site from the construct. The Polyhistidin-tag, flanked with NdeI and NcoI sites, was removed by mutating the NcoI site to NdeI by site directed mutagenesis and restriction digestion with NdeI and religation of the construct. The plasmids pCA24N-adk, pCA24N-eno, pCA24N-fucO, pCA24N-glxK, pCA24N-gph and pCA24N-gpmI were obtained from the ASKA collection[7]. The gene gox0313 was ordered readily cloned in the vector pET16b (BaseClear B.V.), using NdeI and BamHI restriction sites (pTE1453). For the construction of pTE1125, the insert of pBBR1p264-gox1801-ST[8] (which was a kind gift of U. Deppenmeier, Bonn (Germany)) was PCR amplified using the primers MC60 and MC61 (Supplementary Table 6) and cloned into a pET16b derivative using NdeI and KpnI restriction sites. To obtain the expression plasmid for *Cd*SucD (pTE1816), the gene was synthesized codon-optimized (Eurofins Genomics Germany GmbH) and cloned into pTE380[6] using NcoI and SalI restriction sites. Plasmids for the expression of all CETCH-enzymes were as described earlier[6].

Bacterial strains. For cloning purposes, *E. coli* DH5α (Thermo Fisher Scientific) was used. For transformation of the megaWHOP products (see library generation), *E. coli* ElectroMAX DH5α (Thermo Fisher Scientific) were used. For expression of recombinant proteins *E. coli* BL21 (DE3), *E. coli* BL21-AI (Thermo Fisher Scientific) or *E. coli* Rosetta (DE3) pLysS (Novagen Merck) were used. For the expression of biotin-dependent carboxylases, *E. coli* BL21 (DE3) containing the pJZ152 plasmid (encoding for *M. extorquens* biotin ligase) was used (BL21_BirA). For the expression of Nmar0206 we used *E. coli* BL21_GroES/GroEL[6]. For the heterologous expression of acyl-CoA synthetases, an *E. coli* BL21 (DE3) AI Δ*patZ* strain was constructed by using the Quick & Easy *E. coli* Gene Deletion Kit (Gene Bridges GmbH) following the manufacturer's instructions. In brief, in a first step a PCR product from the functional cassette including a kanamycin resistance gene and flanking homology arms was generated using the primers patZ_KO_fw and patZ_KO_rv (Supplementary Table 6). In the next step, the pRedET plasmid containing the recombination genes and a temperature-sensitive origin of replication was transformed into *E. coli* BL21 AI (DE3). To start the recombination process, the expression of the Red/ET recombination genes was induced and the linear PCR product transformed into the cells. To confirm the integration of the Kan-cassette and knock-out of *patZ* in the genome of BL21-AI, single colonies were picked and analyzed by colony PCR using the primers patZ_KO_P1 and patZ_KO_P4 (Supplementary Table 6).

Heterologous expression and purification of recombinant proteins. For the overexpression of recombinant proteins, the corresponding plasmids (Supplementary Table 7) were transformed into chemically competent *E. coli* cells. See Supplementary Table 8 for details on the expression strain. The cells were grown on LB agar plates containing the selective antibiotics (Supplementary Table 8) at 37 °C overnight. Typically, 1 L selective medium was inoculated with the colonies obtained from the overnight culture and grown at 37 °C to an OD_{600} of 0.4 to 1.0, induced with IPTG (and arabinose in the case of ACSs) and grown over night at 21 °C or 25 °C (Supplementary Table 8). Cells were harvested at 6000 × *g* for 12 min at 4 °C and cell pellets were stored at -80 °C until purification of enzymes. Nmar0206 and Nmar0207 were expressed as described earlier[6]. Proteins were purified as described in the following (Supplementary Table 8).

Purification protocol a: Cell pellets were resuspended in two-fold volume of buffer A_{His} (50 mM HEPES, 500 mM NaCl, pH 7.8) containing 0.1 mg mL^{-1} DNase I. The cell suspension was passed through a French pressure cell twice at a pressure of 137 MPa and centrifuged at 100,000 × *g* and 4 °C for 1 h. The supernatant was filtered through a 0.45 µm syringe filter and loaded at a flow rate of 1 mL min^{-1} onto a 1 mL HisTrap™ FF column (GE Healthcare) which had previously been equilibrated with 5 column volumes of buffer A_{His}. The column was washed with 20 column volumes of 90% buffer A_{His} and 10% buffer B_{His} (50 mM Tris/HCl, 500 mM NaCl, 500 mM imidazole, pH 7.8) and the protein was eluted with buffer B_{His}. The fraction containing the eluted enzyme was desalted using 5 mL HiTrap™ Desalting columns (GE Healthcare) and buffer A_{Strep} (50 mM HEPES, 150 mM NaCl, pH 7.8).

Purification protocol b: Cell pellets were resuspended in two-fold volume lysis buffer (20 mM Tris-HCl pH 7.5, 500 mM NaCl, 10% glycerol). Resuspended cells were stored at -20 °C until lysis. Cells were lysed by ultrasonication and the lysate was cleared by ultracentrifugation at 50,000 × *g* for 45 min at 4 °C and subsequently filtered through a 0.45 µm filter. The cleared lysate was loaded onto a 1 mL HisTrap™ FF column (GE Healthcare) and unbound protein was removed with 20 mL of 20 mM Tris-HCl pH 7.5, 500 mM NaCl, 75 mM imidazole. The protein was eluted in 20 mM Tris-HCl pH 7.5, 500 mM NaCl and 500 mM imidazole. The protein from elution fractions was desalted with a HiTrap™ Desalting column (GE Healthcare) in 20 mM Tris-HCl pH 7.5, 200 mM NaCl.

Purification protocol c: Cell pellets were resuspended in two-fold volume of buffer A_{Strep} (50 mM HEPES, 150 mM NaCl, pH 7.8) containing 0.1 mg mL^{-1} DNase I. The cell suspension was passed through a French pressure cell twice at a pressure of 137 MPa and centrifuged at 100,000 × *g* and 4 °C for 1 h. The supernatant was filtered through a 0.45 µm syringe filter and

loaded at a flow rate of 1 mL min^{-1} onto a 1 mL StrepTrap™ HP column (GE Healthcare) which had previously been equilibrated with 5 column volumes of buffer A_{Strep}. The column was washed with 20 column volumes of buffer A_{Strep} and the protein was eluted with buffer A_{Strep} containing 3 mM desthiobiotin.

Purification protocol d: Cell pellets were resuspended in two-fold volume lysis buffer (50 mM Tris-HCl pH 7.5, 150 mM NaCl, 10% glycerol). Resuspended cells were stored at -20 °C until lysis. Cells were lysed by ultrasonication and the lysate was cleared by ultracentrifugation at 50,000 × *g* for 45 min at 4 °C and subsequently filtered through a 0.45 µm filter. The cleared lysate was loaded onto a 1 mL StrepTrap HP (GE Healthcare) and unbound protein was removed with 20 mL of 50 mM Tris-HCl pH 7.5, 150 mM NaCl. The protein was eluted in 50 mM Tris-HCl pH 7.5, 150 mM NaCl and 2.5 mM of desthiobiotin.

Purification protocol e: Cells were resuspended in two-fold volume of lysis buffer (500 mM NaCl, 50 mM HEPES, 10% glycerol, pH 7.8) containing 5 mM $MgCl_2$, 10 µg ml^{-1} DNase and one tablet of Sigma*FAST* Protease Inhibitor Cocktail (Sigma-Aldrich). The cells were lysed by microfluidization (two times at 16,000 psi). The cell lysate was centrifuged at 50,000 × *g* for 1 h at 4 °C. The supernatant was filtered through a 0.45 µm filter. The lysate was mixed with 3 ml Protino Ni-NTA agarose beads (Macherey-Nagel) and incubated on ice for 30-45 min (70 rpm). Afterwards the beads were collected in a gravity column and washed with three column volumes (cv) of lysis buffer. For the removal of unspecific bound proteins the beads were washed with three cv of lysis buffer containing 50 mM imidazole and three cv with lysis buffer containing 75 mM imidazole. The enzymes were eluted in two cv of lysis buffer containing 500 mM imidazole. The collected recombinant protein was concentrated in Amicon Ultra 15 mL Centrifugal Filters (Merck). For desalting, the protein solution was loaded on a HiLoad 16/600 Superdex 200 pg column (GE Healthcare). The desalting/storage buffer contained 200 mM NaCl, 50 mM HEPES and 10% glycerol. For Hbs and Hbd, the buffer contained 500 mM NaCl.

Purification protocol f: Cell pellets were resuspended in two-fold volume of lysis buffer (200 mM MOPS, 100 mM NaCl, pH 7.8) containing 0.1 mg mL^{-1} DNase I. The cell suspension was passed through a French pressure cell at 137 MPa. The lysate was heat precipitated at 65 °C for 10 min and then cooled on ice and centrifuged at 100,000 × *g* and 4 °C for 1 h. The supernatant was filtered through a 0.45 µm syringe filter and used for enzyme assays.

All enzymes were concentrated with Amicon Ultra centrifugal filters (Merck Millipore) with appropriate size cut-offs and concentration was determined using a Nanodrop 2000 spectrophotometer (Thermo Scientific). Enzymes were stored in 20 - 50% glycerol in the

corresponding purification buffer at -20 °C or -80 °C. The storage buffer for Pco and Mco additionally contained FAD (1 µM per µM of enzyme). The storage buffer of Mcm and Ecm additionally contained 2 mM Coenzyme B_{12}. The storage buffer of Nmar0206 additionally contained 2 mM $MgCl_2$. The purity of enzymes was assessed using SDS polyacrylamide gel electrophoresis.

Activity assay of CoA-transferases. Specific activites of acyl-CoA:propionate transferases (*Re*PCT and *Cp*PCT) and 4-OH-butyrate CoA transferase (AbfT) were determined via analysis of the time-dependent formation of glycolyl-CoA using ultra-high performance liquid chromatography coupled high resolution mass spectrometry (UPLC-hrMS). The enzyme assay was performed at 37 °C in a total volume of 60 µL. The reaction mixture contained 200 mM MOPS/KOH pH 7.5, 2 mM acetyl-CoA, 100 µg enzyme and 10 mM to 800 mM glycolate. Aliquots were taken at time points 0.5, 1.0, 1.5 and 2.0 minutes and the reaction was immediately stopped by HCl (1% total concentration). The samples were centrifuged at 17,000 × *g* at 4 °C and the supernatant used for UPLC-hrMS analysis.

Activity assay of acyl-CoA synthetases. To determine specific activities of acyl-CoA synthetases, a coupled spectrophotometric assay to measure AMP formation was used. The ATP hydrolysis reaction was measured coupled to ADP regeneration by myokinase and ATP regeneration by pyruvate kinase (PK) with phosphoenolpyruvate (PEP) and subsequent reduction of pyruvate to lactate by lactic dehydrogenase (LDH). The oxidation of NADH by LDH was followed spectrophotometrically at 340 nm. The assay was performed at 30 °C and typically contained 100 mM MOPS/KOH (pH 7.8), 5 mM $MgCl_2$, 2.5 mM ATP, 15 U mL^{-1} pyruvate kinase, 23 U mL^{-1} lactic dehydrogenase, 2.5 mM PEP, 200 µg mL^{-1} myokinase, 1 mM coenzyme A, 0.4 mM NADH, 2 µg mL^{-1} ACS/GCS and 1 - 200 mM glycolate.

Activity assay of carboxylases. Activity of glycolyl-CoA carboxylase (GCC) was determined spectrophotometrically at 37 °C in three different ways.

The ATP hydrolysis reaction was measured coupled to ATP regeneration by pyruvate kinase (PK) with phosphoenolpyruvate (PEP) and subsequent reduction of pyruvate to lactate by lactic dehydrogenase (LDH). The oxidation of NADH by LDH was followed spectrophotometrically at 340 nm. The reaction mixture (200 µL) typically contained 100 mM MOPS/KOH pH 7.8, 5 mM ATP, 50 mM $KHCO_3$, 2.5 mM phosphoenolpyruvate, 15 U mL^{-1} pyruvate kinase,

23 U mL^{-1} lactic dehydrogenase, 0.4 mM NADH, 7.5 mM $MgCl_2$, 2 mM glycolyl-CoA and 40 µg mL^{-1} GCC.

To measure carboxylation activity, spectrophotometric assays at 365 nm were performed coupling the product formation (tartronyl-CoA) to its subsequent reduction via tartronic semialdehyde to glycerate by use of tartronyl-CoA reductase (TCR). This coupling reaction was analogous to an activity assay for acetyl-CoA carboxylase[9]. The reaction mixture (200 µL) typically contained 100 mM MOPS/KOH pH 7.8, 1.7 mg mL^{-1} TCR, 50 mM $KHCO_3$, 0.6 mM NADPH, 5 mM $MgCl_2$, 100 µg mL^{-1} GCC, 0.8 - 2 mM glycolyl-CoA and 0.8 - 5 mM ATP. For determination of the ratio of ATP hydrolysis to carboxylation, the TCR-coupled assay was used under ATP-limiting conditions (0.8 mM) and the ratio of ATP-hydrolysis to carboxylation was calculated from the delta absorption values.

For determination of kinetic parameters of GCC variants, we analyzed the time-dependent formation of tartronyl-CoA using ultra-high performance liquid chromatography coupled high resolution mass spectrometry (UPLC-hrMS). The assays contained 100 mM MOPS/KOH pH 7.8, 50 mM $KHCO_3$, 6 mM $MgCl_2$, 3 mM ATP, 0.03 - 0.3 mg mL^{-1} GCC and 0.1 - 1.6 mM glycolyl-CoA. Aliquot samples were withdrawn, quenched with 1% HCl, centrifuged at 17,000 × *g* for 20 min at 4 °C and analyzed by UPLC-hrMS.

Activity assay of acyl-CoA reductases. The kinetics of tartronyl-CoA reduction of *Ca*MCR (TCR) and *Ery*MCR were determined spectrophotometrically at 365 nm following the oxidation of NADPH. Per molecule tartronyl-CoA, two molecules of NADPH are oxidized by MCR, which was taken into account for the calculation of specific activities. The measurements were carried out at 37 °C in 100 mM MOPS/KOH pH 7.5, 5 mM $MgCl_2$, 0.4 mM NADPH, 115 µg mL^{-1} *Ca*MCR or 88 µg mL^{-1} *Ery*MCR and 0.01 - 2 mM tartronyl-CoA.

Activity assay of dehydrogenases. The specific activities of FucO and Gox0313 with ethylene glycol were determined spectrophotometrically at 37 °C and 340 nm. The assay contained 100 mM MOPS/KOH pH 7.8, 155 µg mL^{-1} FucO or 35 µg mL^{-1} Gox0313, 2 mM NAD^+ and 10 - 2000 mM ethylene glycol. The specific activity of PduP with glycol aldehyde was measured spectrophotometrically at 37 °C and 340 nm and the assay contained 100 mM MOPS/KOH pH 7.8, 11 µg mL^{-1} PduP, 0.5 mM CoA, 1 mM NAD^+ and 50 mM glycolaldehyde dimer.

Activity assay of 2-phosphoglycolate phosphatase. Phosphoglycolate phosphatase (Pgp) was assayed in 100 mM MOPS/KOH pH 7.8, 5 mM $MgCl_2$ and 2 mM 2-phosphoglycolate with 7 µg mL^{-1} Pgp at 37 °C. Aliquot samples were taken at time points 0 min, 1 min and 10 min and quenched with HCl (1% end concentration). The samples were analyzed using the Phosphate colorimetric kit (Sigma-Aldrich) following the manufacturer's instructions and the specific activity was calculated from the enzyme- and time-dependent release of P_i.

Activity assay of glycerate kinase. The activity of glycerate kinase (GlxK) was measured spectrophotometrically at 340 nm and 37 °C. The assay contained 100 mM MOPS/KOH pH 7.8, 1 mM ATP, 5 mM $MgCl_2$, 0.4 mM NADH, 2.5 mM phosphoenolpyruvate, 0.5 mM glycerate, 15 U mL^{-1} pyruvate kinase, 23 U mL^{-1} lactate dehydrogenase and 4 µg mL^{-1} GlxK.

Activity assay of phosphoglycerate mutase. Activity of phosphoglycerate mutase (Gpm) was measured spectrophotometrically at 340 nm and 37 °C. The assay contained 100 mM MOPS/KOH pH 7.8, 1 mM ADP, 5 mM $MgCl_2$, 0.4 mM NADH, 66 µg mL^{-1} enolase, 15 U mL^{-1} pyruvate kinase, 23 U mL^{-1} lactate dehydrogenase, 1 mM 3-phosphoglycerate and 5 µg mL^{-1} Gpm.

Activity assays of enzymes of the CETCH cycle. Activities of all enzymes of the CETCH cycle were measured as described previously [6].

Michaelis-Menten kinetics. Michaelis-Menten kinetics were typically calculated from 18 independent activity measurements (six different substrate concentrations in triplicates) using non-linear regression analysis in GraphPad Prism 8.0.

Avidin gel shift assay. To confirm full biotinylation of biotin-dependent carboxylases, we performed avidin gel shift assays as described previously for streptavidin[10]. In brief, 10 µM of carboxylase was mixed with non-reducing SDS-PAGE buffer (final concentrations 2% SDS, 10% glycerol, 60 mM Tris-HCl pH 6.8) and incubated for 5 min at 100 °C. 10 µM of avidin (Santa Cruz Biotechnology) in PBS was added and loaded onto a gradient SDS gel (Mini-PROTEAN® TGX™ 4-20%, Bio-Rad) after 5 min incubation at RT. The gel was run for 90 min at 100 V in Rotiphorese® SDS-PAGE buffer (Roth) and stained afterwards with GelCode™ Blue Safe Protein Stain (Thermo Scientific).

Circular dichroism (CD) spectroscopy. Protein denaturation curves were obtained by monitoring the ellipticity at 218.5 nm using a Jasco-J-815 CD spectropolarimeter equipped with a Jasco PTC-423S temperature controller. 0.3 mg ml^{-1} purified protein was loaded in a 1mm Quartz Suprasil (Helma) cuvette with 15 mM HEPES at pH 7.8 and 45 mM KCl. A bandwidth of 3.41 nm and D.I.T of 2 s was used with a heating rate of 1 °C min^{-1} in a temperature range of 20 - 80 °C. CD spectra of each protein were measured from 205 - 250 nm at 20 °C with a scanning speed of 100 nm min^{-1}. T_m determination was done using the Jasco Spectra Manager 2.06 software.

Microfluidic device fabrication. Microfluidic chips were prepared from poly-(dimethylsiloxane) (PDMS, Sylgard 184) from SU8-3000 negative photoresist (MicroChem Corp) molds produced using standard soft-lithography procedures[11]. The surfaces of the microfluidic channels were treated with fluoro-silane (Aquapel, Aquapel) before use.

Microfluidic device operation. All the microfluidic workflows (devices and flow rates) for performing short-term or long-term multiplexed kinetics were as previously described[12]. The microfluidic devices were placed and held on an inverted microscope (IX71, Olympus) and connected to either Nemesys syringe pumps (Cetoni) or a pressure driven pump (Fluigent, MFCS-4C) via PTFE tubing (Fisher Scientific; inner diameter (ID) of 0.3 mm; outer diameter (OD) of 0.76 mm) to control the flow in the microfluidic devices. Droplets were produced in fluorinated oil (Novec7500, 3M) and stabilized against coalescence by a perfluoropolyether-polyethyleneglycol block-copolymer surfactant (PFPE-PEG-PFPE), synthesized as previously described[13]. The optical set up for fluorescence detection was similar to that reported previously[12]. Data acquisition (DAQ) and control were performed by a DAQ card (National Instruments) executing a program written in LabVIEW (National Instruments). The data acquisition rate for the system was 200 kHz.

Microfluidic assays with purified GCC. To establish a microfluidic assay to screen for better GCC variants, the coupled spectrophotometric assay of GCC with TCR to monitor carboxylation activity was transferred into water-in-oil (w/o) droplets with purified GCC using a short-term multiplexed kinetics workflow[12]. Substrate solutions containing all substrates except for glycolyl-CoA and the purified GCC were encapsulated in 30 pL w/o droplets and a glycolyl-CoA solution was injected into these droplets to start the reaction. The final concentrations in the droplets were 100 mM MOPS/KOH pH 7.8, 1 - 5 mM ATP, 2.5 - 7.5 mM

$MgCl_2$, 1 mM NADPH, 50 mM $KHCO_3$, 1 mM glycolyl-CoA, 80 µg mL^{-1} GCC, 400 µg mL^{-1} *Ca*MCR and 30, 60, 90 or 120 µM sulforhodamine B.

Microfluidic assays with single encapsulated *E. coli* cells. For single-cell microfluidic encapsulation, *E. coli* BL21 (DE3) cells were freshly transformed with PCC, GCC M3 or the randomized libraries 1_1, 1_2 and 1_3, and grown on selective agar plates overnight. 25 mL of selective LB medium was inoculated to an OD_{600nm} of approx. 0.1 and the cells were grown to an OD_{600nm} of 0.4 to 0.6. Protein expression was induced by the addition of 0.2 mM IPTG. The cells were grown for 3 h or overnight, subsequently harvested by centrifugation (10 min at 2500 × *g*) and washed three times with 100 mM MOPS/KOH pH 7.8. In the case of experiments with GCC libraries, the library expressing cells were pooled before centrifugation. After determination of OD_{600nm} the cells were diluted to a final in-droplet OD_{600nm} of 0.05 to achieve a droplet occupancy by cells of 5% to 10%, assuring that droplets containing cells only contain a single cell. Sulforhodamine B was added at varying concentrations (10 µM to 150 µM) to the solutions. A separate substrate and cell lysis solution was prepared containing (final in-droplet concentration) 100 mM MOPS/KOH pH 7.8, 0 - 5 mM ATP, 5 - 10 mM $MgCl_2$, 1 mM NADPH, 50 mM $KHCO_3$, 0.1 x CelLytic B (Sigma Aldrich), 1 mM glycolyl-CoA and 400 µg mL^{-1} *Ca*MCR. The conditions for cell lysis were as described previously[14]. Cells were encapsulated in 30 pL droplets, incubated at 37 °C and reinjected for analysis over time using a long-term multiplexed kinetics workflow[12].

Mass spectrometry of CoA esters (UPLC-hrMS). The measurements of CoA esters were done using an Agilent 6550 iFunnel Q-TOF LC-MS system equipped with an electrospray ionization source set to positive ionization mode.

Compounds were separated on an RP C18 column (50 mm x 2.1 mm, particle size 1.7 µm, Kinetex EVO C18, Phenomenex) using a mobile phase system comprised of 50 mM ammonium formate pH 8.1 (A) and methanol (B). Chromatographic separation was carried out using the following gradient condition at a flow rate of 250 µL min^{-1}: 0 min 2.5% B; 1 min 2.5% B, 6 min 95% B; 6.25 min 95% B; 6.35 min 2.5% B; 7 min 2.5% B. Capillary voltage was set at 3.5 kV and nitrogen gas was used for nebulizing (20 psig), drying (13 L min^{-1}, 225 °C) and sheath gas (12 L min^{-1}, 400 °C). The TOF was calibrated using an ESI-L Low Concentration Tuning Mix (Agilent) before measurement (residuals less than 2 ppm for five reference ions) and was recalibrated during a run using 922 *m/z* as reference mass. MS data

were acquired with a scan range of 500 - 1200 *m/z*. LC-MS data were analyzed using MassHunter Qualitative Analysis and TOF Quantitative Analysis (Agilent).

Mass spectrometry of organic acids. Glycerate and malate were derivatized according to a method described earlier[15]. In brief, 10 µL of sample was mixed with 10 µL 150 mM 1-(3-Dimetheylaminopropyl)-3-ethylcarbodiimide (EDC), 10 µL 250 mM 3-nitrophenylhydrazine (3-NPH), and 10 µL of 7.5% pyridine in methanol in a 1.5 mL reaction tube. The reaction was incubated at 30 °C for 30 min. After incubation, the samples were centrifuged at 13,000 x *g* for 1 min and the supernatant was transferred into HPLC vials. UPLC-MS/MS analyses were performed on an Agilent 6495B Triple Quad LC/MS system equipped with an electrospray ionization source.

The analytes were separated on an RP-18 column (50 mm x 2.1 mm, particle size 1.8 µm, Kinetex EVO C18, Phenomenex) kept at 40 °C using a mobile phase system comprised of 0.1% formic acid in water (A) and acetonitrile (B). The gradient was as follows: 0 min 5% B; 1 min 5% B, 6 min 95% B; 6.5 min 95% B; 7 min 5% B at a flow rate of 250 µL min^{-1}. Samples were held at 15 °C and injection volume was 5 µL. MS/MS data were acquired in negative MRM mode. Capillary voltage was set at 3 kV and nitrogen gas was used as nebulizing (25 psig), drying (11 L min^{-1}, 130 °C) and sheath gas (12 L min^{-1}, 400 °C). The dwell time and fragmentor voltage were 20 ms and 380 V, respectively. Optimized collision energy used for the 3-NPH derivatized-glycerate (240 *m/z* → 137 *m/z*) and malate (403 *m/z* → 137 *m/z*) was 22 V and 40 V respectively. LC-MS data were analyzed and quantified using MassHunter Qualitative Navigator and QQQ Quantitative Analysis software (Agilent).

Mass spectrometry of phosphoglycerate. Phosphoglycerate was measured using UPLC-high resolution MS. The analysis was performed using an Agilent 6550 iFunnel Q-TOF LC-MS system equipped with an electrospray ionization source set to negative ionization mode. Compounds were separated on a Phenomenex Luna NH_2 (30 mm x 2 mm, particle size 3 µm, 100 Å) and eluted by a binary gradient mobile phase system comprised of 20 mM ammonium acetate pH 9.3/acetonitrile 95:5 (solvent A) and acetonitrile (solvent B). Chromatographic separation was carried out using the following gradient condition at a flow rate of 250 µL min^{-1}: 0 min 85% B; 3.5 min 0% B, 7 min 0% B; 7.5 min 85% B; 8 min 85% B. The column oven and autosampler were maintained at 10 °C. Injection volume was set to 1 µL. The ESI-MS was operated with the following parameters: Capillary voltage: 3.5 kV, Nebulizer: 20 psig, drying gas (N_2): 13 L min^{-1} at 225 °C, sheath gas (N_2): 12 L min^{-1} at 400 °C). The QTOF mass detector

was calibrated prior to measurement using an ESI-L Low Concentration Tuning Mix (Agilent) with residuals and corrected residuals less than 2 ppm and 1 ppm respectively. MS data were acquired with a scan range of 50 - 600 *m/z* and peaks were analyzed and integrated using the Agilent MassHunter Qualitative Analysis software.

Optimization of ATP regeneration for *in vitro* reconstruction of the TaCo pathway. For the optimization of ATP regeneration for *in vitro* reconstruction of the TaCo pathway, we tested different systems, including two types of polyphosphate kinase (PPK2-I from *Sinorhizobium meliloti* for regeneration of ATP from ADP and polyphosphate, and PPK2-II from *Acinetobacter johnsonii* for regeneration of ADP from AMP and polyphosphate)[16], myokinase and creatine phosphokinase (CPK). The assays contained 100 mM MOPS/KOH pH 7.8, 5 mM ATP, 10 mM $MgCl_2$, 2 mM coenzyme A, 2 mM NADPH, 50 mM $KHCO_3$, 1 mM glycolate, 150 µg mL^{-1} GCS, 608 µg mL^{-1} GCC and 1120 µg mL^{-1} TCR. Additionally, the assays contained 20 - 500 mM phosphocreatine (CP), 6.7 U mL^{-1} creatine phosphokinase (CPK), 20 mM polyphosphate (PP), 33 µg mL^{-1} polyphosphate kinase 2-I (PPK2-I) in combination with 133 µg mL^{-1} polyphosphate kinase 2-II (PPK2-II) or 67 µg mL^{-1} myokinase (and variations thereof). The assay was started with the addition of ATP, samples were withdrawn at different time points and immediately quenched with 1% HCl. The samples were centrifuged at 17,000 × *g* for 20 min at 4 °C and analyzed via UPLC-MS/MS for glycerate using the derivatization method (see below).

Spectrophotometric assay of the TaCo pathway. The initial assay contained 100 mM MOPS/KOH pH 7.8, 10 mM $MgCl_2$, 0.4 mM NADPH, 50 mM $KHCO_3$, 0.15 mg mL^{-1} GCS, 0.56 mg mL^{-1} GCC M4 and 1.1 mg mL^{-1} TCR. Then, first 20 mM glycolate were added, then 1 mM coenzyme A and the assay was then started with the addition of 5 mM ATP. The decrease in NADPH absorption at 340 nm was followed spectrophotometrically.

***In vitro* reconstruction of the TaCo pathway from 2-PG.** For the reconstruction of the TaCo pathway starting from 2-phosphoglycolate (2-PG), assays were run at 37 °C. The assays initially contained 100 mM MOPS/KOH pH 7.8, 10 mM $MgCl_2$, 2 mM NADPH, 50 mM $NaH^{13}CO_3$, 2 mM coenzyme A, 200 mM phosphocreatine, 20 mM polyphosphate, 10 mM glucose-6-phosphate, 4.8 U mL^{-1} G6PDH, 0.19 mg mL^{-1} PPKII-2, 4.8 U mL^{-1} creatine kinase, 0.03 mg mL^{-1} Pgp, 0.58 mg mL^{-1} GlxK, 0.46 mg mL^{-1} GCS, 0.69 mg mL^{-1} GCC M4 and 1.07 mg mL^{-1} TCR. The assay was started with the addition of 2.5 mM phosphoglycolate and

5 mM ATP, samples were withdrawn at different time points and immediately quenched with 1% HCl. The samples were centrifuged at 17,000 × *g* for 20 min at 4 °C and analyzed via UPLC-MS/MS for 2-PGA.

Supplementary Figures

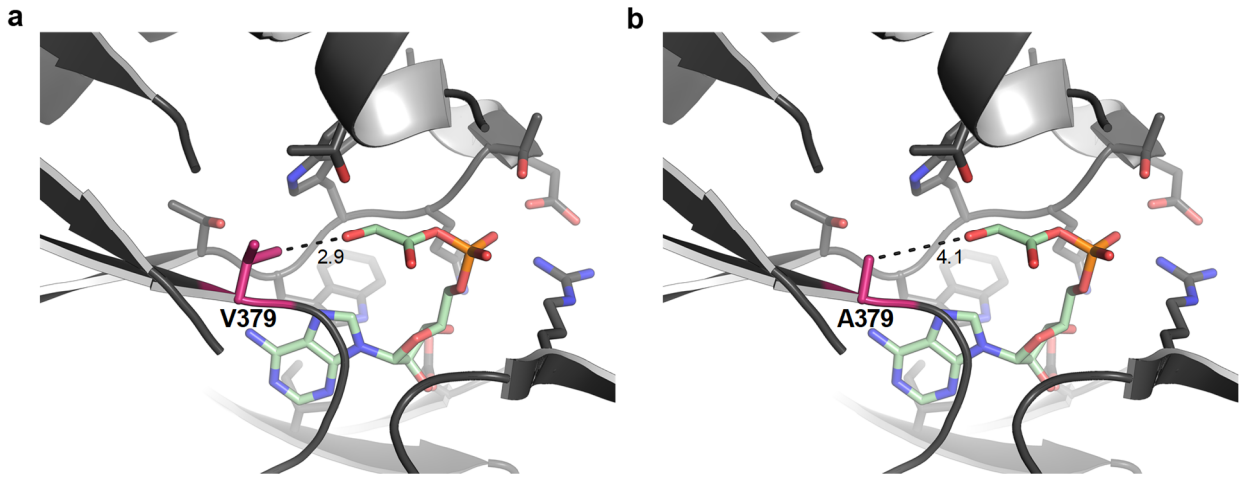

Supplementary Figure 1. Active site homology model for acetyl-CoA synthetase 1 of *Erythrobacter* sp. NAP1. The homology model is based on the crystal structure of an acetyl-CoA synthetase from *S. enterica* (PDB 2P2B). The residue targeted for mutagenesis is shown in pink. The reaction intermediate glycolyl-AMP was modelled into the active site based on the position of an adenosine-5'-monophosphate-propyl ester (mimicking the acetyl-AMP reaction intermediate of *S. enterica* ACS) bound in PDB 2P2B. Distances are given in Å. (**a**) In the wild type *Ery*ACS1, the hydroxyl group of the glycolyl moiety would be in an unfavorable close contact to the non-polar V379. (**b**) In the V379A mutant of *Ery*ACS1 (GCS) the active site provides more space to presumably accommodate glycolyl-AMP better.

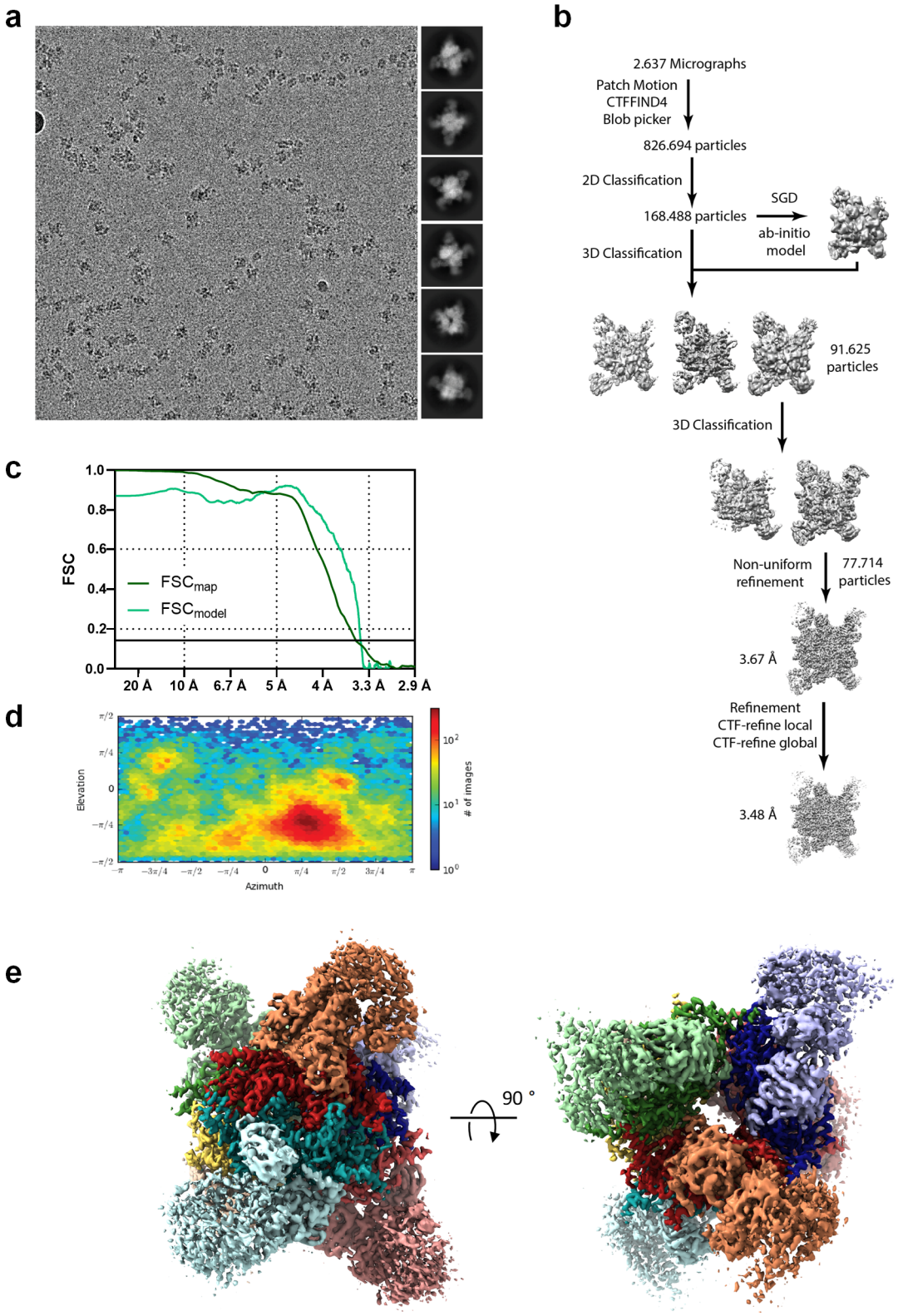

Supplementary Figure 2. Cryogenic electron microscopy (Cryo-EM) data collection and analysis for *Me*PCC. (**a**) A representative cryo-EM micrograph collected on an FEI Glacios microscope, operated at 200 kV and equipped with a K2 camera and representative reference-free 2D class averages. (**b**) Overview of the cryo-EM data processing scheme. (**c**) FSC_{map}: Gold-standard fourier shell correlation (FSC) plot from the final round of refinement in cryoSPARC. FSC_{model}: Model vs. map FSC for the final Phenix real space refined model. (**d**) Angular distribution of the particles used for the final round of refinement. (**e**) 3.48 Å resolution cryo-EM structure of *Me*PCC.

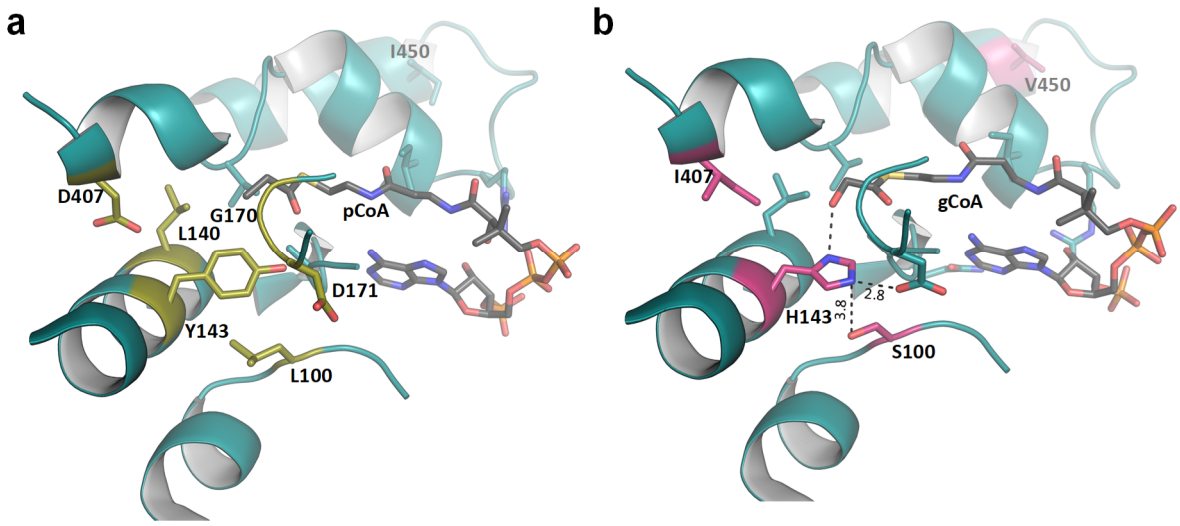

Supplementary Figure 3. Active site comparison of propionyl-CoA carboxylase of *M. extorquens* and engineered glycolyl-CoA carboxylase. (**a**) Cryo-EM structure of propionyl-CoA carboxylase of *M. extorquens* (*Me*PCC) active site (PDB 6YBP). Propionyl-CoA (pCoA) was modelled according to the position of methylmalonyl-CoA in PDB 1ON3 (**b**) Cryo-EM structure of engineered glycolyl-CoA carboxylase active site (PDB 6YBQ). Glycolyl-CoA (gCoA) was modelled according to the position of methylmalonyl-CoA in PDB 1ON3 with additional manual fitting that reflects the new active site architecture and coordination distances.
Residues targeted during rational design of the active site are colored in yellow. Actual active site changes in the GCC M4 and M5 mutants are colored in pink. Potential new hydrogen bonds are depicted as dashed lines. Distances are given in Å. The Y143H mutation is likely engaging in hydrogen bonding with the hydroxyl group of glycolyl-CoA. The L100S mutation is assumed to fix H143 in a rotamer conformation facilitating hydrogen bonding interaction with glycolyl-CoA. The I450V mutation is located in an α-helix nearby and may impact distances within the active site or at the interface with the biotin carboxylase subunit.
In addition to the four mutations in and around the active site, GCC M5 features an additional mutation outside of the active site (W502R), which is located at the rotational symmetry of the enzyme oligomer.

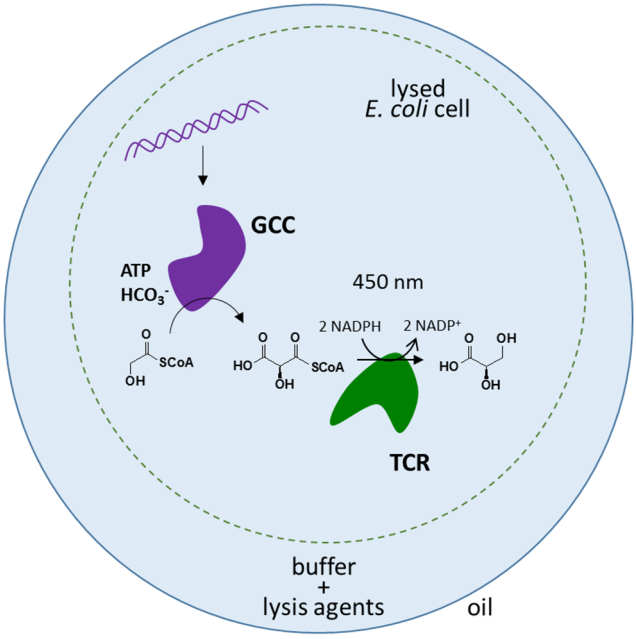

Supplementary Figure 4. Scheme of microfluidic assay for activity measurements of glycolyl-CoA carboxylase (GCC). Either purified GCC or single *E. coli* cells expressing variants of GCC were encapsulated in water-in-oil droplets. ATP, $KHCO_3$ and glycolyl-CoA were provided as substrates. The formation of the carboxylation product tartronyl-CoA was coupled to a decrease in NADPH fluorescence by its reduction to glycerate by the coupling enzyme TCR. In order to screen for GCC variants with decreased ATP hydrolysis to carboxylation ratios, the amount of ATP within the droplets was limited.

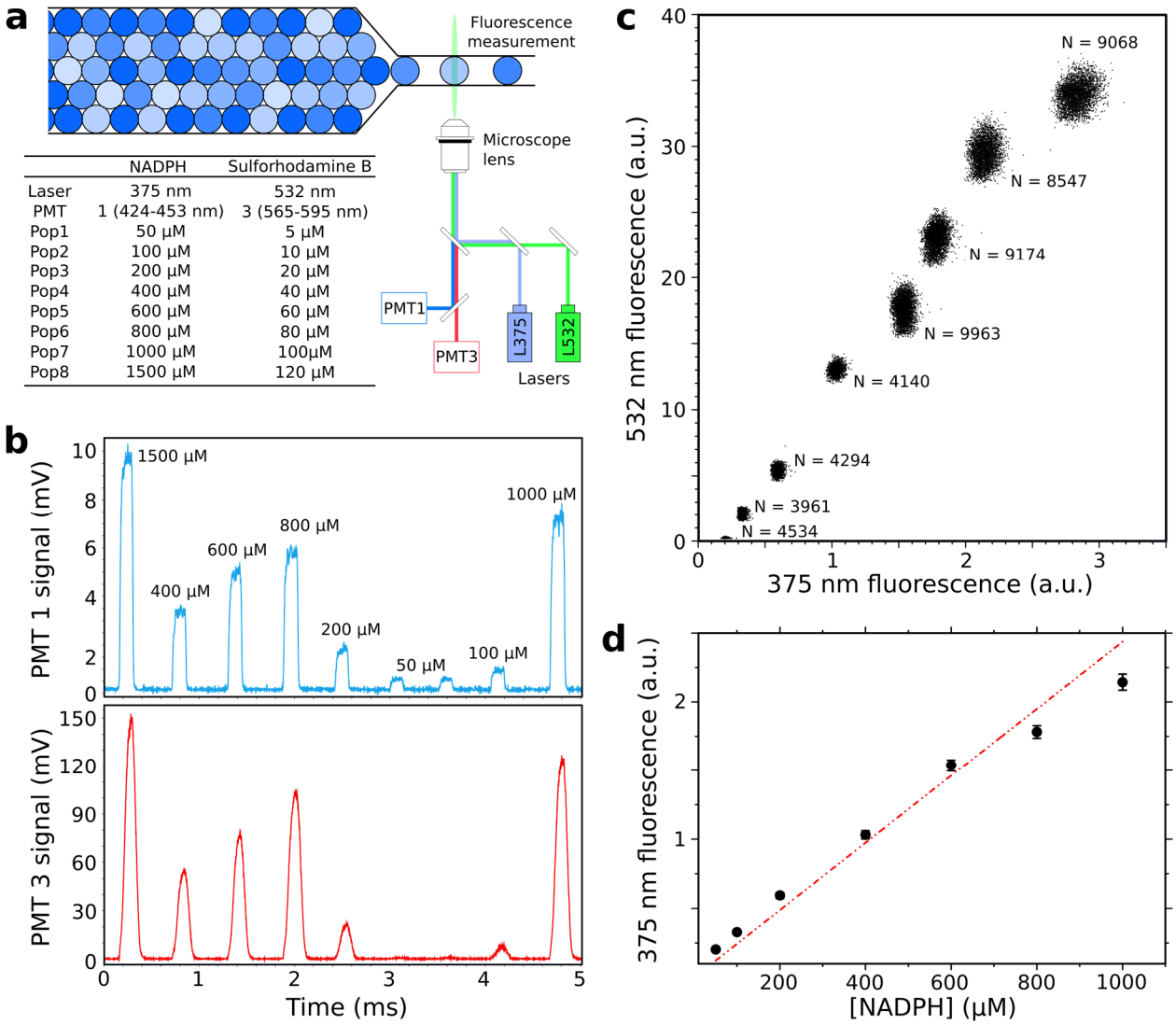

	NADPH	Sulforhodamine B
Laser	375 nm	532 nm
PMT	1 (424-453 nm)	3 (565-595 nm)
Pop1	50 µM	5 µM
Pop2	100 µM	10 µM
Pop3	200 µM	20 µM
Pop4	400 µM	40 µM
Pop5	600 µM	60 µM
Pop6	800 µM	80 µM
Pop7	1000 µM	100µM
Pop8	1500 µM	120 µM

Supplementary Figure 5. Microfluidic fluorescence measurements. (**a**) Scheme of the microfluidic optical set up. Single droplet fluorescence was measured at kHz frequencies inside microchannels using the combination of two lasers (375 and 532 nm) with two photomultiplier tubes (PMT1 and PMT3). The optical set up allowed the detection of either NADPH fluorescence (enzymatic read out) or sulforhodamine B fluorescence (barcoding). To make a NADPH fluorescence calibration, an 8-bit emulsion of w/o droplets containing different concentrations of NADPH and sulforhodamine B was produced and analysed. (**b**) Time sequence of the signal of PMT1 (NADPH) and PMT3 (sulforhodamine B) for the corresponding 8-bit emulsion. (**c**) 2D plot showing the fluorescence distribution of the corresponding 8-bit emulsion. (**d**) NADPH concentration versus fluorescence level using the microfluidic set up. Data represent mean ± SD for n ≥ 3961 measured droplets.

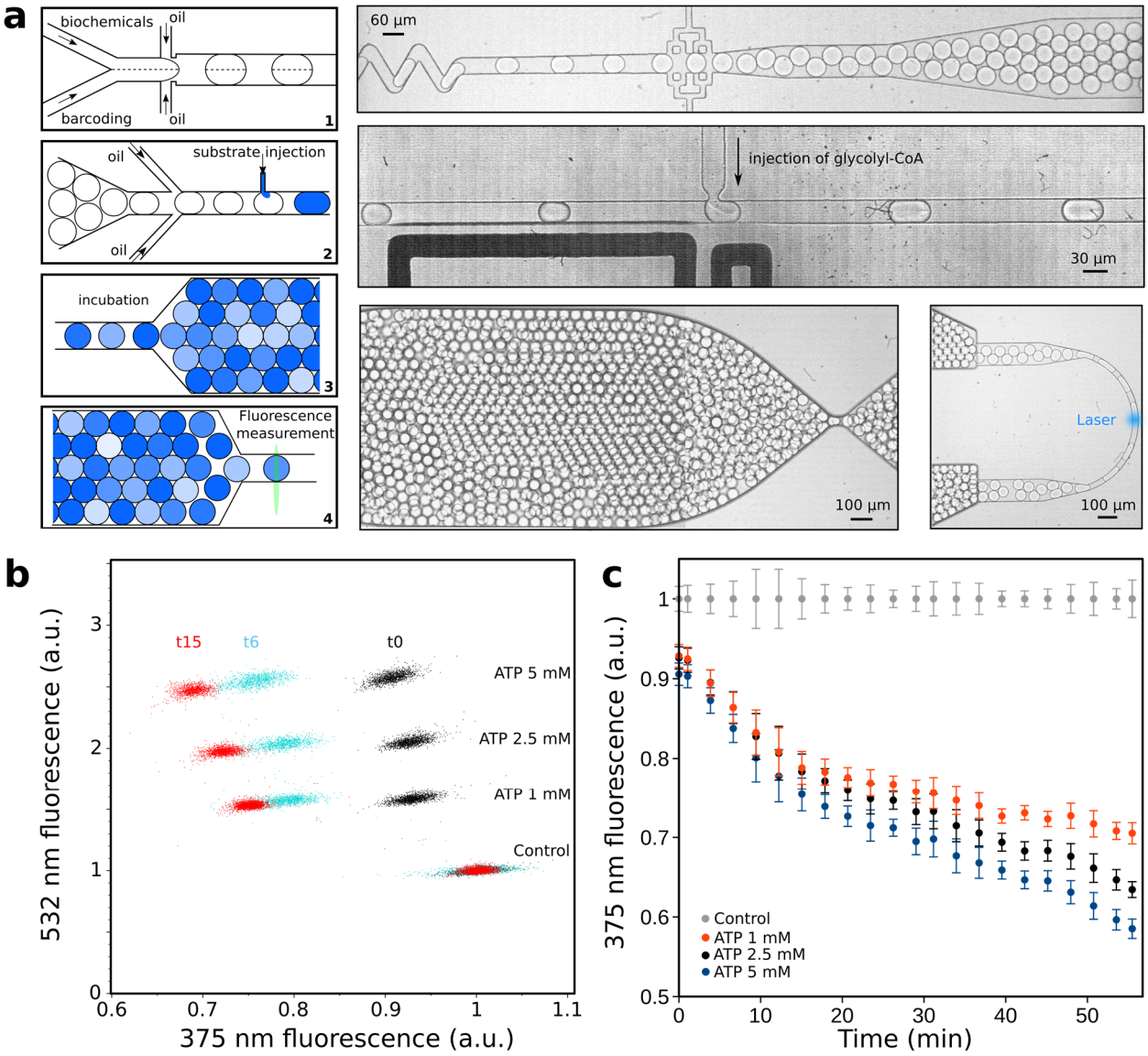

Supplementary Figure 6. Microfluidic assay for activity measurements of variant 3 of glycolyl-CoA carboxylase (GCC M3) with on chip incubation. (**a**) Microfluidic workflow: droplets were produced (1), collected off-chip and reloaded in a kinetic device (2). Glycolyl-CoA was picoinjected (2) and droplets were incubated on-chip (3). NADPH fluorescence was measured over time at different measurement loops (4). (**b**) 2D plot showing NADPH oxidation over time in four different populations of droplets. Except for population 1, all populations contained 53 µg mL^{-1} GCC M3. Population 1: 1 mM ATP, 30 µM sulforhodamine B; population 2: 1 mM ATP, 60 µM sulforhodamine B; population 3: 2.5 mMATP, 90 µM sulforhodamine B; population 4: 5 mM ATP, 120 µM sulforhodamine B. (**c**) The NADPH oxidation over time was dependent on the ATP concentration within the droplets. Data points represent mean ± SD (n=1500 measured droplets).

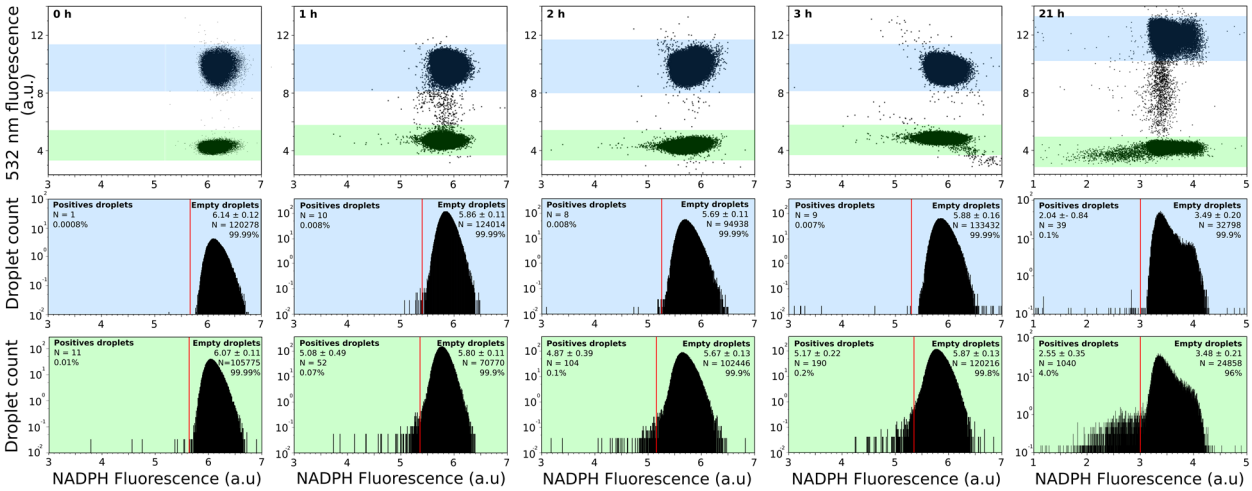

Supplementary Figure 7. Microfluidic assay with droplets containing single cells. *E. coli* cells expressing either PCC WT or GCC M3 were encapsulated into droplets with all assay components. The droplets with PCC WT contained 60 µM sulforhodamine B and the droplets with GCC M3 contained 20 µM sulforhodamine B as a barcoding. After encapsulation of single cells, the droplets were collected, incubated at 37 °C and fluorescence was measured directly after encapsulation, and 1 h, 2 h, 3 h and 21 h after encapsulation. 2D and 1D histograms show the fluorescence distribution of the 2-bit emulsion over time. The blue population corresponds to PCC WT cells and the green population corresponds to GCC M3 cells. The red line threshold gates negative and positive droplets and is defined as the mean value of the main population (empty droplets) minus 4 σ (standard deviation).

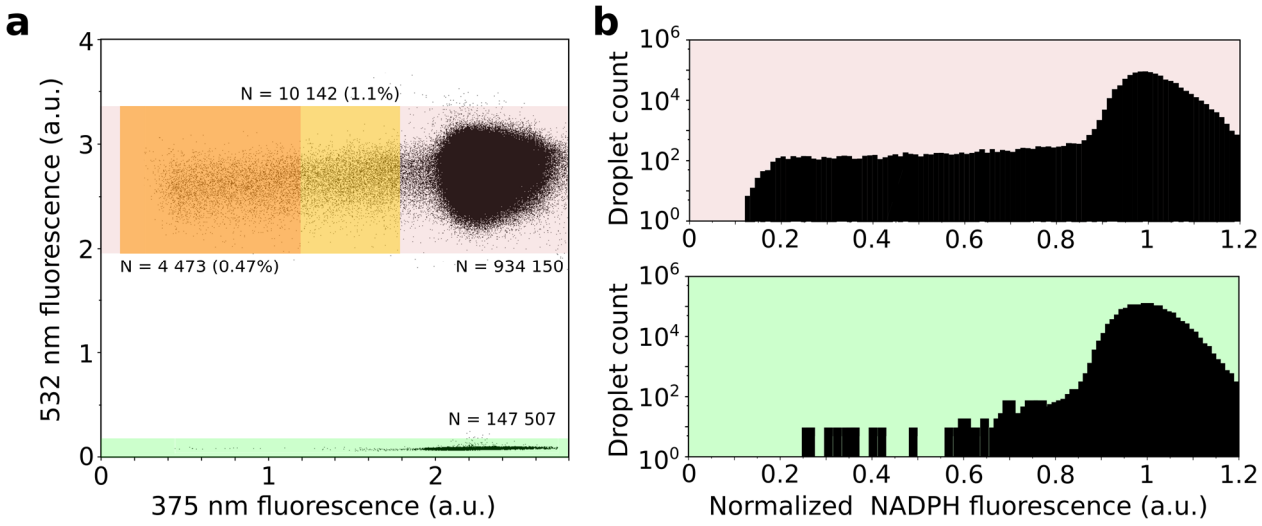

Supplementary Figure 8. Microfluidic assay for cells expressing variants of glycolyl-CoA carboxylase (GCC). *E. coli* cells expressing variants of GCC were encapsulated into water-in-oil droplets including lysis agents, reaction substrates and sulforhodamine B as coding dye (droplets with cells expressing GCC M3 2 µM and with cells expressing GCC variants 20 µM). The library contained variants that produce more carboxylation product (tartronyl-CoA) which led to more NADPH oxidation and therefore higher decrease in NADPH fluorescence signal. 2D (**a**) and 1D (**b**) histograms show the fluorescence distribution of the 2-bit emulsion after overnight incubation. The green population corresponds to PCC M3 cells and the pink population corresponds to cells expressing GCC variants. The yellow gate corresponds to active variants (defined as the mean of the main population minus 4 σ) and the orange gate corresponds to variants showing a higher activity than GCC M3. Note that only 10% of the droplets contain cells, therefore 0.47% of droplets containing more active variants corresponds to 4.7% of more active variants in total.

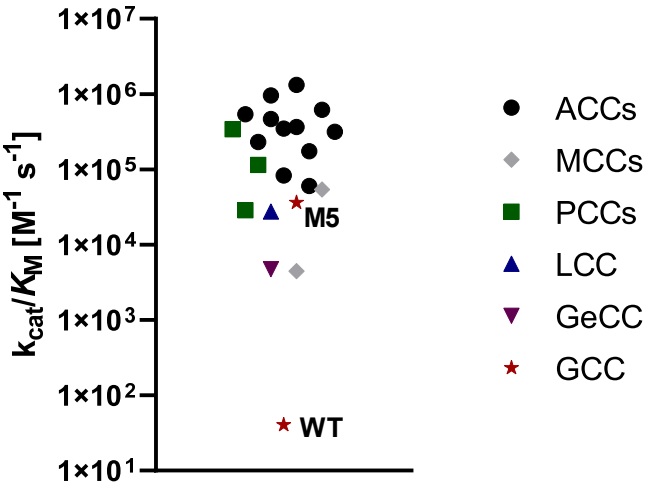

Supplementary Figure 9. Catalytic efficiencies of different biotin-dependent acyl-CoA carboxylases. Data for acetyl-CoA carboxylases (ACCs), methyl-crotonyl-CoA carboxylases (MCCs) and propionyl-CoA carboxylases (PCCs) were taken from[6]. Data for long-chain acyl-CoA carboxylase (LCC) were calculated from[17]. Data for geranoyl-CoA carboxylase (GeCC) were calculated from[18]. All data represent catalytic efficiencies of the respective enzymes with their respective physiological substrate, except for GCC WT (the evolutionary starting point of GCC) and GCC M5, which represent the catalytic efficiency of these enzymes with glycolyl-CoA.

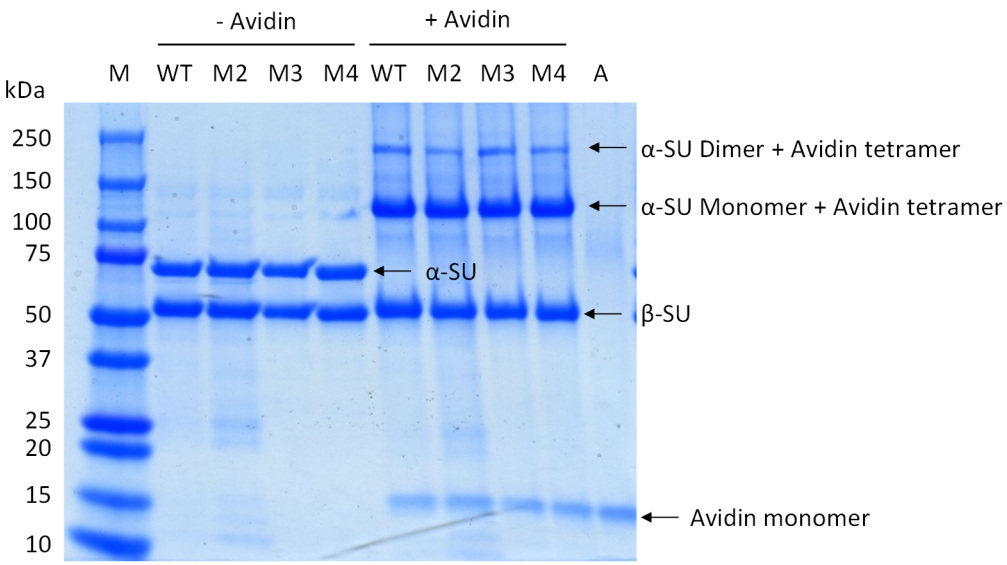

Supplementary Figure 10. Avidin gel shift assay of to test for full biotinylation of propionyl-CoA carboxylase of *M. extorquens* (WT) and different engineered glycolyl-CoA carboxylase (GCC) variants. The gel is representative of two independent experiments with similar results. M: molecular weight standard, WT: PCC *M. extorquens* wildtype, M2: GCC M2, M3: GCC M3, M4: GCC M4, A: avidin, α-SU: α-subunit of PCC/GCC, β-SU: β-subunit of PCC/GCC. Theoretical molecular weight: α-SU 72 kDa, β-SU: 58 kDa, α-SU monomer + avidin tetramer 140 kDa, α-SU dimer + avidin tetramer 212 kDa, avidin monomer 17 kDa.

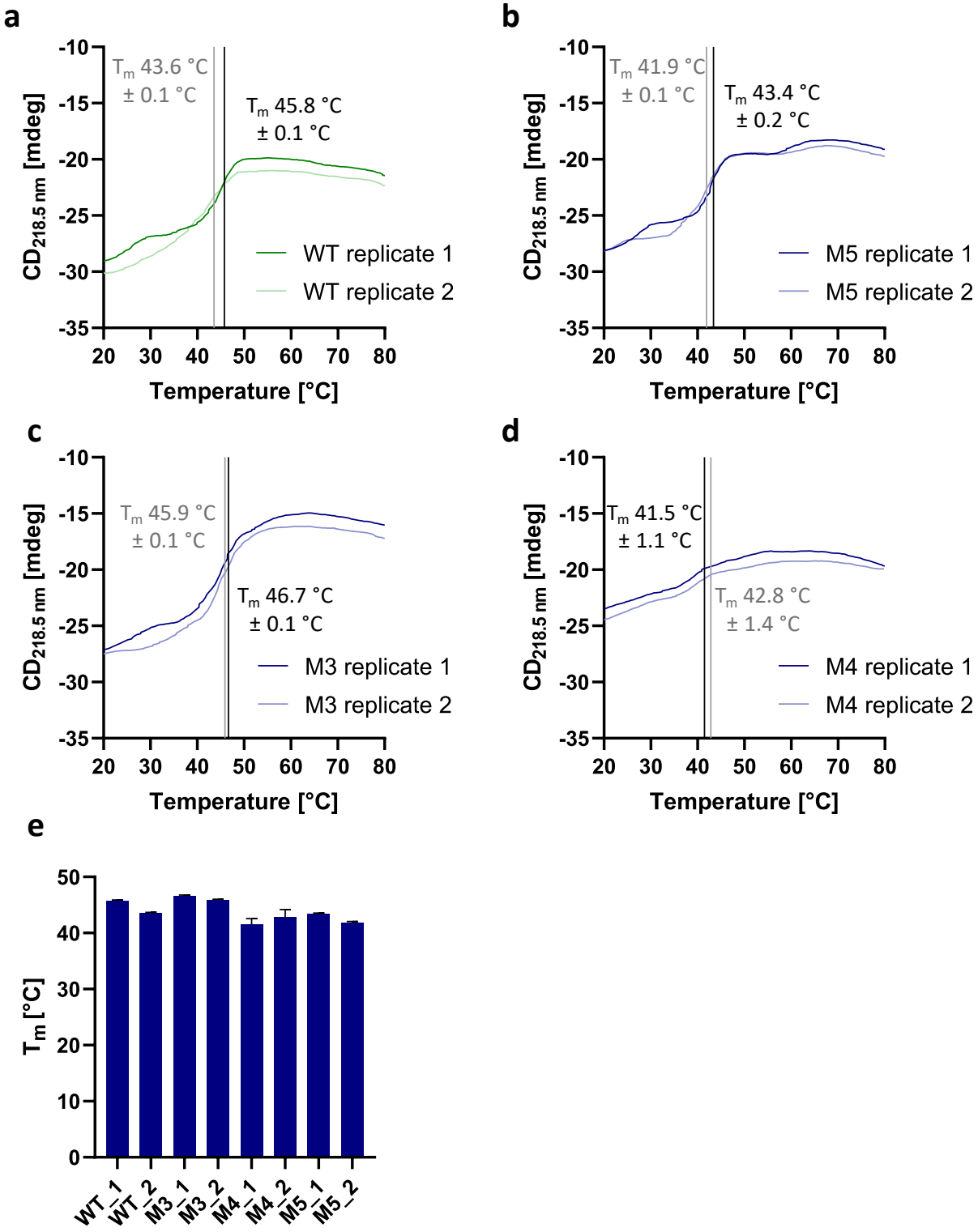

Supplementary Figure 11. Circular dichroism spectroscopy for melting point determination of GCC variants. Two technical replicates are shown for each enzyme variant. (**a**) *Me*PCC WT. (**b**) GCC M5. (**c**) GCC M3. (**d**) GCC M4. (**e**) Comparison of melting temperatures (T_m) for the different variants. Shown are the calculated values for the inflection points of each individual curve (a-d), error bars represent the standard error of the fit. Calculations were performed using the Jasco Spectra Manager software.

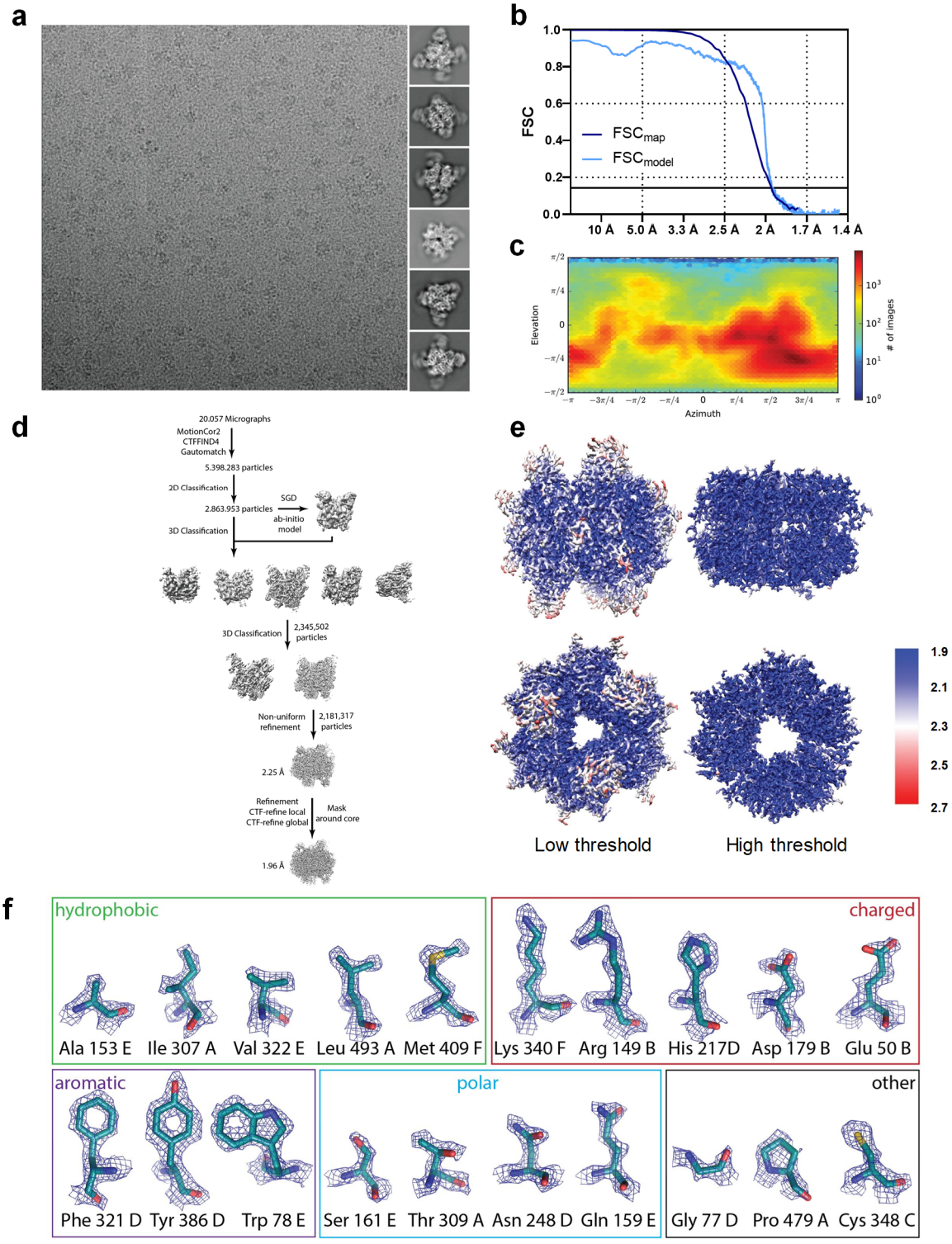

Supplementary Figure 12. Cryogenic electron microscopy (Cryo-EM) data collection and analysis for GCC M5. (**a**) A representative cryo-EM micrograph collected on an FEI Titan Krios microscope, operated at 300 kV and equipped with a K3 camera and representative reference-free 2D class averages. (**b**) Tight: Gold-standard fourier shell correlation (FSC) plot from the final round of refinement in cryoSPARC. Masked: Model vs. map FSC for the final Phenix real space refined model. (**c**) Angular distribution of the particles used for the final round of refinement. (**d**) Overview of the cryo-EM data processing scheme. (**e**) Local resolution analysis of GCC M5. Maps show variation in local resolution of the central β-core of the complex, as estimated by cryoSPARC. Left: Low density threshold image, showing the presence of the BCCP domain. Right: High-density threshold image, showing the high resolved β-domains of the molecule (**f**) Representative side-chains of the complex (in stick representation) and surrounding electron density map. Maps are displayed as a mesh using a contour level of up to 2 Å around the atoms. Subunits and residue numbers are specified.

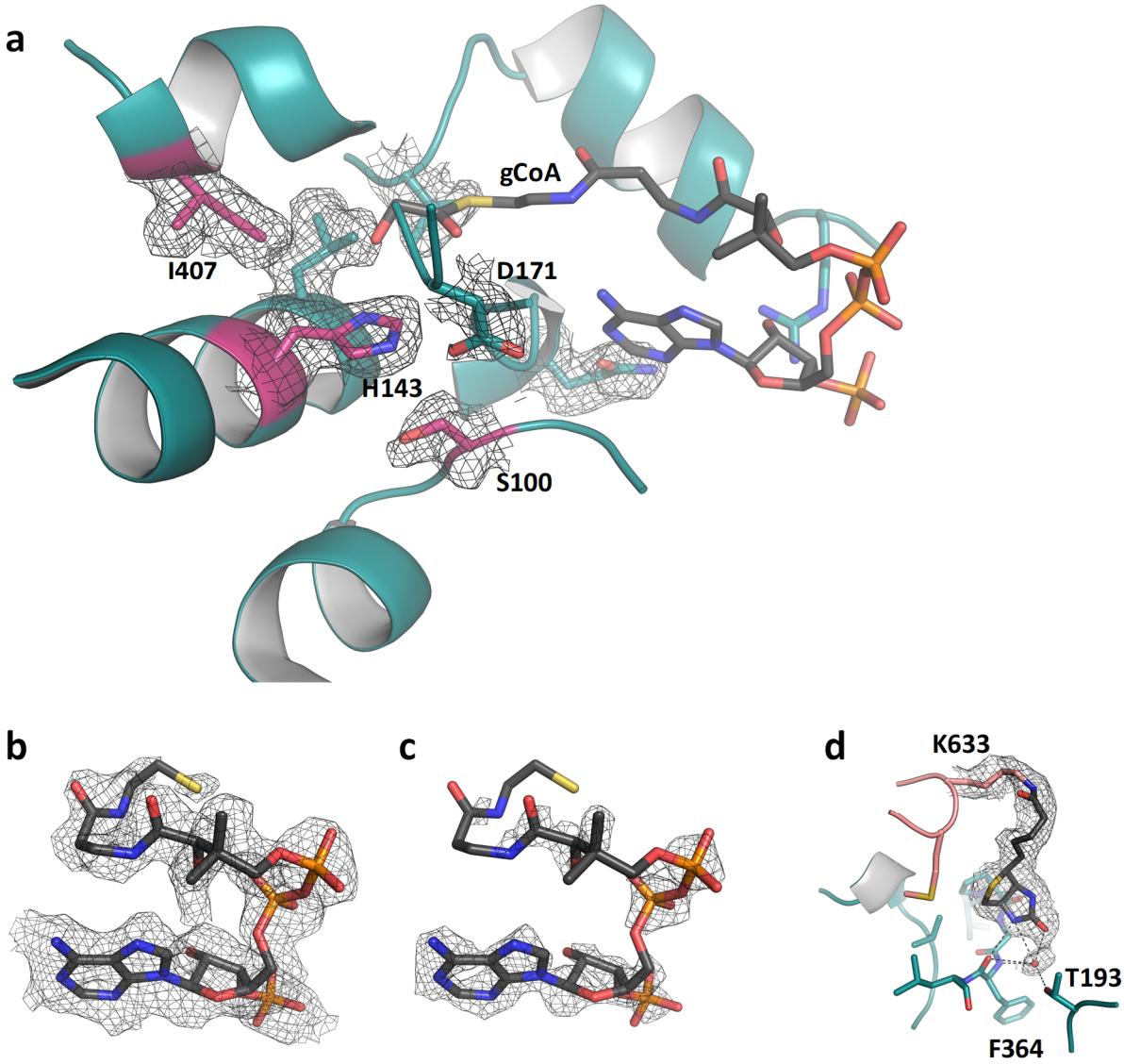

Supplementary Figure 13. Electron density maps for GCC M5 as obtained by cryo-EM. (**a**) Active site of GCC M5. Rationally introduced mutations are highlighted in pink. Glycolyl-CoA (gCoA) was modelled based on the position of methylmalonyl-CoA in PDB 1ON3 with additional manual fitting that reflects the GCC M5 active site architecture and coordination distances. (**b**) Electron density map at low contour level for coenzyme A as present in the cryo-EM structure. (**c**) Electron density map at high contour level for coenzyme A emphasizing the tight binding of the adenosyl moiety and the flexibility of the pantetheine arm. (**d**) Biotin cofactor covalently bound to Lys633 of GCC M5 α-subunit (salmon). β-subunits are shown in teal. Possible hydrogen bonds are depicted as dashed lines.

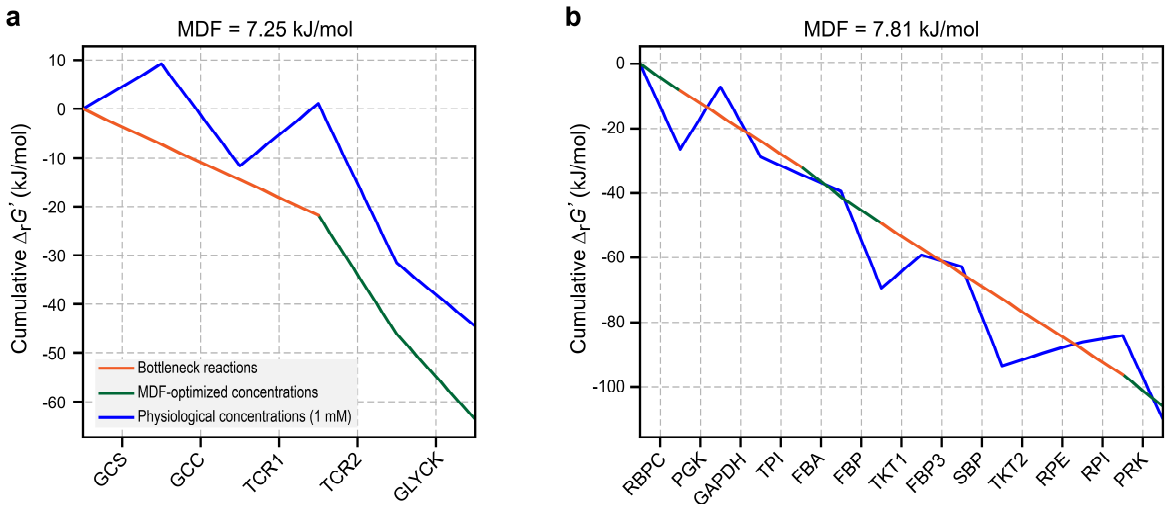

Reaction	$\Delta_r G'^{o}$ kJ/mol	$\Delta_r G'^{m}$ kJ/mol	$\Delta_r G'$ kJ/mol	Shadow price
GCS	9.25	9.25	-7.25	0.33
GCC	-20.86	-20.86	-7.25	0.33
TCR1	29.78	12.67	-7.25	0.33
TCR2	-32.68	-32.68	-24.39	0.00
GLYCK	-12.85	-12.85	-17.45	0.00

Reaction	$\Delta_r G'^{o}$ kJ/mol	$\Delta_r G'^{m}$ kJ/mol	$\Delta_r G'$ kJ/mol	Shadow price
RBPC	-26.39	-26.39	-8.30	0.00
PGK	19.32	19.32	-7.81	0.21
GAPDH	-4.47	-21.59	-7.81	0.21
TPI	-5.58	-5.58	-7.81	0.07
FBA	-22.39	-5.28	-9.49	0.00
FBP	-12.77	-29.88	-8.16	0.00
TKT1	10.19	10.19	-7.81	0.07
FBP3	-20.84	-3.72	-7.81	0.07
SBP	-13.45	-30.57	-7.81	0.07
TKT2	3.88	3.88	-7.81	0.07
REP	3.39	3.39	-7.81	0.14
RPI	2.08	2.08	-7.81	0.07
PRK	-25.88	-25.88	-9.74	0.00

Supplementary Figure 14. Optimized thermodynamic profiles and Max-min Driving Force (MDF) of the tartronyl-CoA pathway (a) and the Calvin-Benson-Bassham (CBB) cycle (b). Blue lines correspond to $\Delta_r G'^{o}$ values of pathway reactions at pH 7, ionic strength 0.25 M and pMg 3. Green lines correspond to $\Delta_r G'$ values of pathway reactions after optimization of metabolite concentration towards maximal MDF (see Methods). The orange lines represent the predicted bottleneck reactions (positive shadow prices).

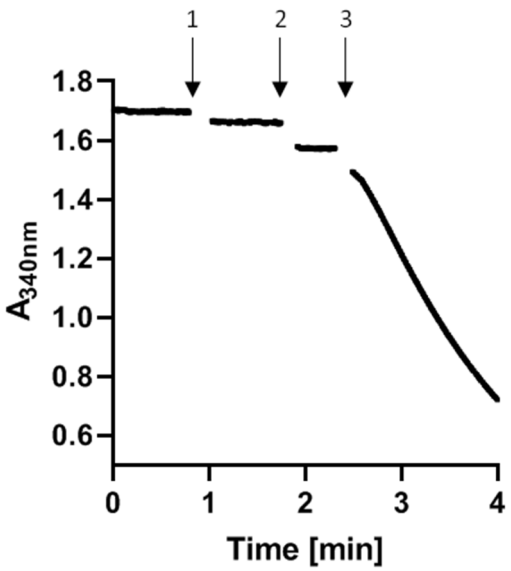

Supplementary Figure 15. Spectrophotometric assay for activity assessment of the complete TaCo pathway. The assay contained 100 mM MOPS/KOH, 10 mM $MgCl_2$, 0.4 mM NADPH, 50 mM $KHCO_3$, 0.15 mg mL^{-1} GCS, 0.56 mg mL^{-1} GCC M4, 1.1 mg mL^{-1} TCR. 1: addition of 20 mM glycolate, 2: addition of 1 mM coenzyme A, 3: addition of 5 mM ATP. Data shown are representative of three independent experiments.

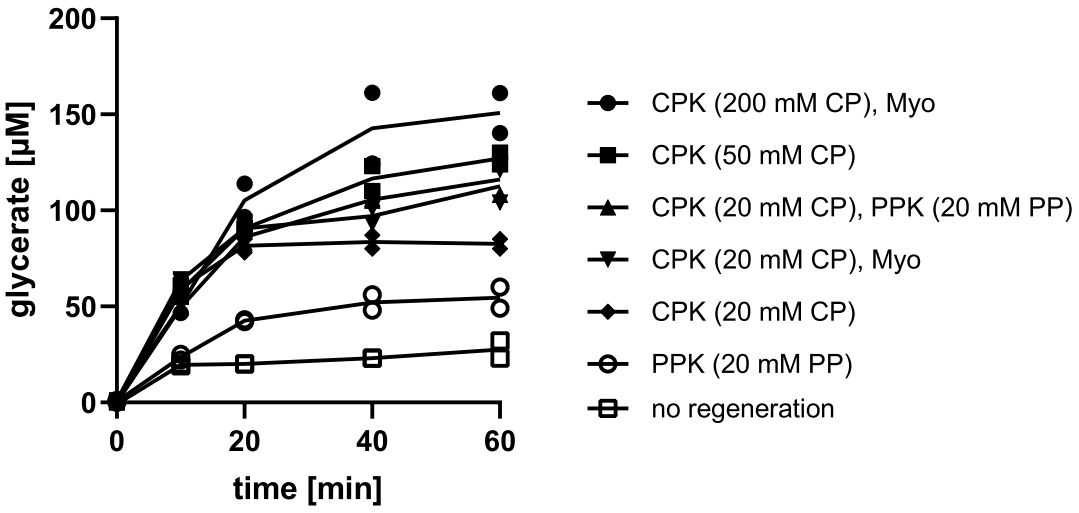

Supplementary Figure 16. Optimization of ATP regeneration for *in vitro* operation of the TaCo pathway. The assays contained 100 mM MOPS/KOH pH 7.8, 5 mM ATP, 10 mM $MgCl_2$, 2 mM coenzyme A, 2 mM NADPH, 50 mM $KHCO_3$, 1 mM glycolate, 150 µg mL^{-1} GCS, 608 µg mL^{-1} GCC and 1120 µg mL^{-1} TCR. Additionally, the assays contained 20 - 500 mM phosphocreatine (CP), 6.7 U mL^{-1} creatine phosphokinase (CPK), 20 mM polyphosphate (PP), 33 µg mL^{-1} polyphosphate kinase 2-I (PPK2-I) in combination with 133 µg mL^{-1} polyphosphate kinase 2-II (PPK2-II) or 67 µg mL^{-1} myokinase (and variations thereof as indicated in the legend). Shown is mean and individual data points of two independent experiments.

a

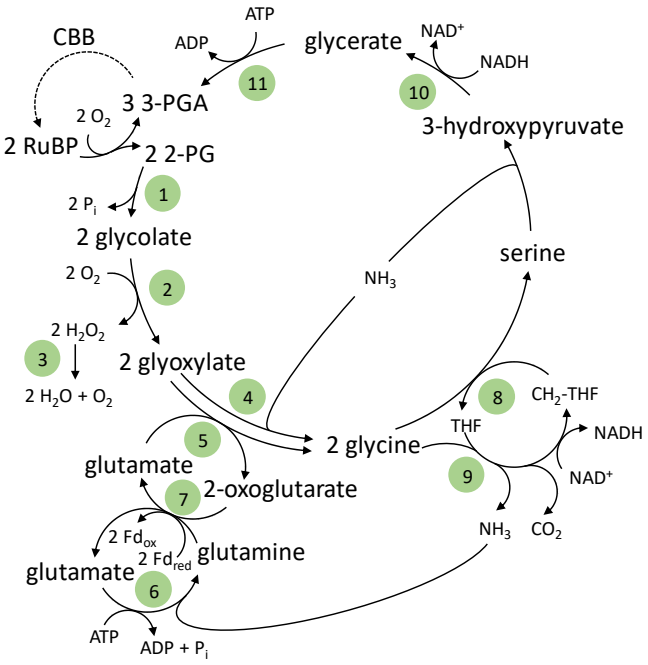

#	enzyme
1	phosphoglycolate phosphatase
2	glycolate oxidase
3	catalase
4	serine/glyoxylate aminotransferase
5	glutamate/glyoxylate aminotransferase
6	glutamine synthetase
7	glutamine/oxoglutarate aminotransferase
8	serine hydroxymethyl transferase
9	glycine decarboxylase
10	hydroxypyruvate reductase
11	glycerate kinase

b

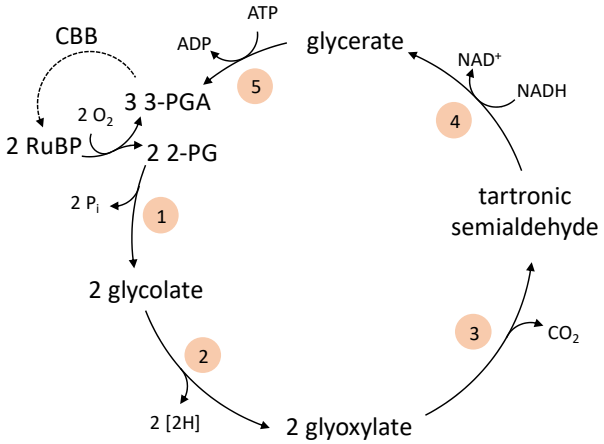

#	enzyme
1	phosphoglycolate phosphatase
2	glycolate dehydrogenase
3	glyoxylate carboligase
4	tartronic semialdehyde reductase
5	glycerate kinase

c

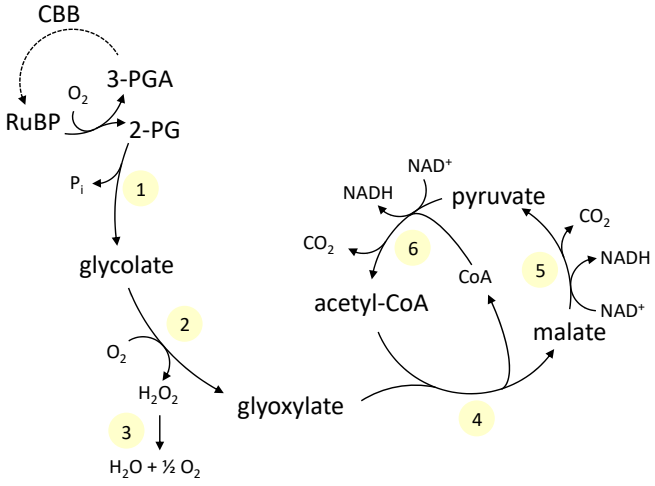

#	enzyme
1	phosphoglycolate phosphatase
2	glycolate oxidase
3	catalase
4	malate synthase
5	NAD-malic enzyme
6	pyruvate dehydrogenase

d

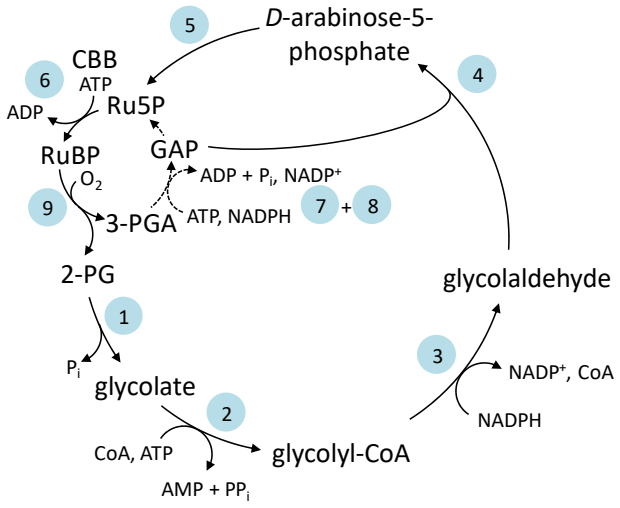

#	enzyme
1	phosphoglycolate phosphatase
2	glycolyl-CoA synthetase
3	glycolyl-CoA reductase
4	fructose-6-phosphate aldolase
5	arabinose-5-phosphate isomerase
6	phosphoribulokinase
7	phosphoglycerate kinase
8	glyceraldehyde-3-phosphate dehydrogenase
9	RuBisCO

e

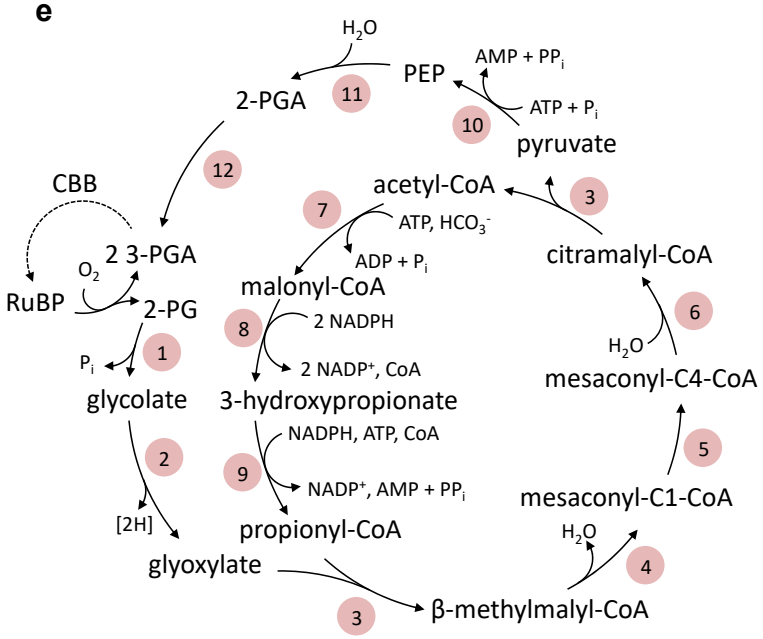

#	enzyme
1	phosphoglycolate phosphatase
2	glycolate dehydrogenase
3	malyl-CoA/β-methylmalyl-CoA/citramalyl-CoA lyase
4	mesaconyl-C1-CoA hydratase
5	mesaconyl-CoA transferase
6	mesaconyl-C4-CoA hydratase
7	acetyl-CoA carboxylase
8	malonyl-CoA reductase
9	propionyl-CoA synthase
10	pyruvate phosphate dikinase
11	enolase
12	phosphoglycerate mutase

f

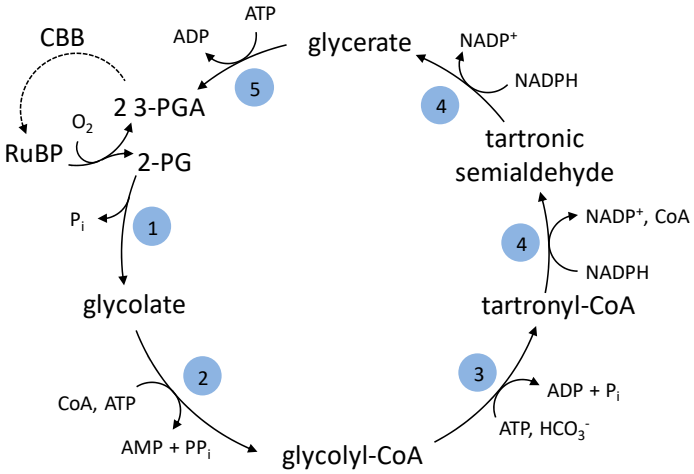

#	enzyme
1	phosphoglycolate phosphatase
2	glycolyl-CoA synthetase
3	glycolyl-CoA carboxylase
4	tartronyl-CoA reductase
5	glycerate kinase

Supplementary Figure 17. Photorespiratory C_2-pathway and synthetic bypasses. (**a**) Natural (canonical) photorespiration of C_3-plants. (**b**) Glycerate bypass[19]. Notably, the physiological electron acceptor of glycolate dehydrogenase (2) is not known. (**c**) Glycolate oxidation pathway[20]. A variation was introduced into Tobacco plants with glycolate dehydrogenase instead of glycolate oxidase[21]. (**d**) Arabinose-5-phosphate shunt[1]. (**e**) 3-OH-propionate bypass[22]. (**f**) tartronyl-CoA pathway (this work).
Abbreviations: CBB: Calvin-Benson-Bassham cycle, RuBP: ribulose-1,5-bisphoshate, THF: tetrahydrofolate, CH_2-THF: methylenetetrahydrofolate, Fd_{red}: reduced ferredoxin, Fd_{ox}: oxidized ferredoxin

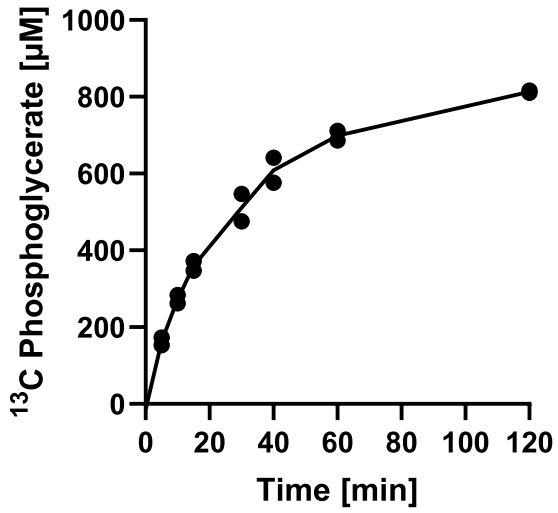

Supplementary Figure 18. ^{13}C-phosphoglycerate produced by the TaCo pathway from 2-phosphoglycolate and ^{13}C bicarbonate. The experiment demonstrated that the TaCo pathway is able to convert RuBisCO's oxygenation product, 2-phosphoglycolate, into phosphoglycerate through direct carboxylation (indicated by the incorporation of $H^{13}CO_3^-$). Furthermore, the experiment showed that (*R*)-glycerate is the product of the TaCo pathway, because *E. coli* GlxK only accepts the (*R*)-stereoisomer of glycerate[23-25]. Shown are the results of two independent experiments as mean and individual data points.

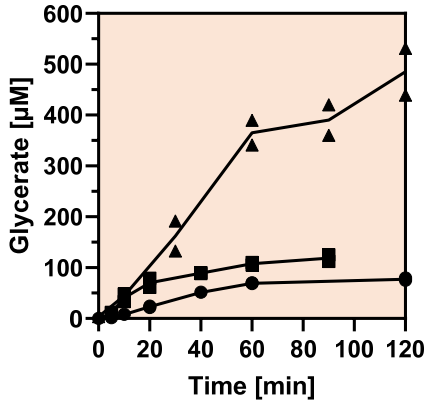

	●	■	▲
Experiment	**EG_1**	**EG_2**	**EG_3**
EG oxidation	FucO	Gox0313	Gox0313
ATP regeneration	n/a	CPK	CPK
phosphocreatine conc. [mM]	n/a	10	200
NADH oxidase [µg µL^{-1}]	n/a	0.04	0.08
final glycerate conc. [µM]	77	119	485
production rate (60 min) [nmol min^{-1} mg^{-1}]*	0.4	0.6	2.1

Supplementary Figure 19. Optimization of experiments for ethylene glycol conversion to glycerate by the ethylene glycol module coupled to the tartronyl-CoA pathway. In the course of optimization, the enzyme for ethylene glycol oxidation was changed from FucO to Gox0313 and ATP regeneration by creatine phosphokinase (CPK) as well as NAD^+ regeneration by a water-forming NADH oxidase was included. The conditions for each experiment are depicted in the table. Shown are the results of two independent experiments each. Final glycerate concentration and production rate represent the mean of the two independent experiments shown. EG_1: ethylene glycol experiment 1, EG_2: ethylene glycol experiment 2, EG_3: ethylene glycol experiment 3.
* Production rate is based on the concentration of TaCo enzymes. n/a - not applicable.

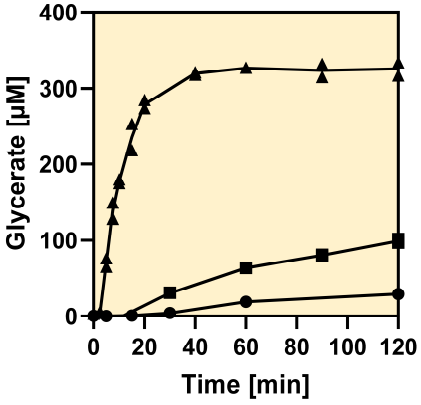

	●	■	▲
Experiment	**CT_1**	**CT_2**	**CT_3**
NADPH regen.	formate DH	formate DH	glucose DH
ATP regen.	PPK2-I, PPK2-II	PPK2-I, PPK2-II	CPK, Myo
polyphosphate conc. [mM]	20	20	n/a
phosphocreatine conc. [mM]	n/a	n/a	100
TaCo addition	@start	after 120 min	after 120 min
SucD	*C. kluyveri*	*C. kluyveri*	*C. difficile*
propCoA (start) [µM]	200	1000	170
final glycerate conc. [µM]	31	105	331
rate of TaCo [nmol min^{-1} mg^{-1}]*	0.1	0.4	4.8

Supplementary Figure 20. Optimization of experiments for coupling of the tartronyl-CoA pathway to the CETCH cycle for the production of glycerate. In the course of optimization, the NADPH regeneration was changed from using formate dehydrogenase (formate DH) to glucose dehydrogenase (glucose DH), the ATP regeneration was changed from using polpyphosphate kinase (PPK2-I and PPK2-II) to creatine phosphokinase (CPK). The enzyme for succinyl-CoA reduction in the CETCH cycle was changed from SucD from *Clostridium kluyveri* to the homolog from *Clostridioides diffile* to reduce side reactivity with glycolyl-CoA. Shown are the results of two independent experiments each. Final glycerate concentration and rate of TaCo represent the mean of the two independent experiments shown. CT_1: CETCH-TaCo experiment 1, CT_2: CETCH-TaCo experiment 2, CT_3: CETCH-TaCo experiment 2.
* The rate is based on the concentration of TaCo enzymes. n/a - not applicappble**.**

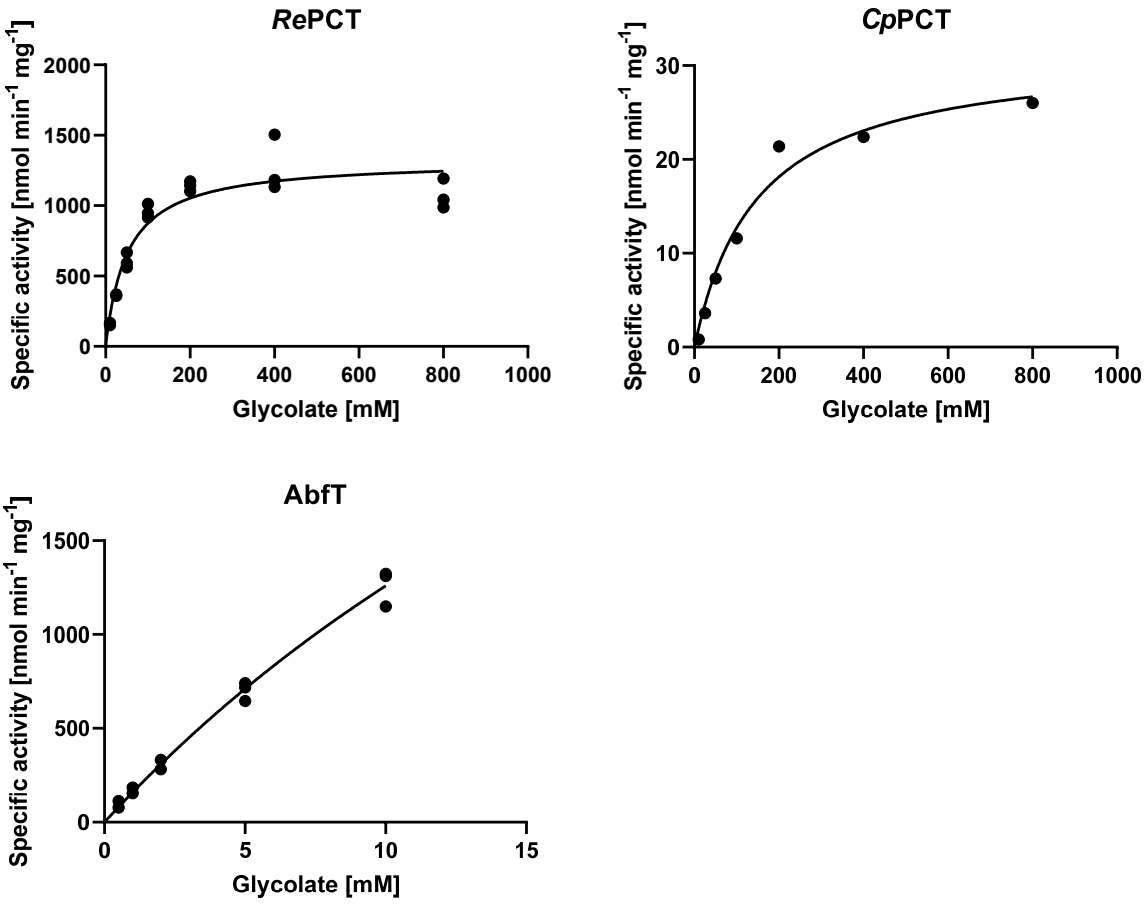

Supplementary Figure 21. Michaelis-Menten kinetics of different acyl-CoA transferases. *Re*PCT: propionyl-CoA transferase of *Ralstonia eutropha*, *Cp*PCT: propionyl-CoA transferase of *Clostridium propionicum*, AbfT: 4-OH-butyryl-CoA transferase of *Clostridium aminobutyricum*. Each data point for n=3 (n=1 for *Cp*PCT) independent measurements is shown. The data were analysed using nonlinear regression.

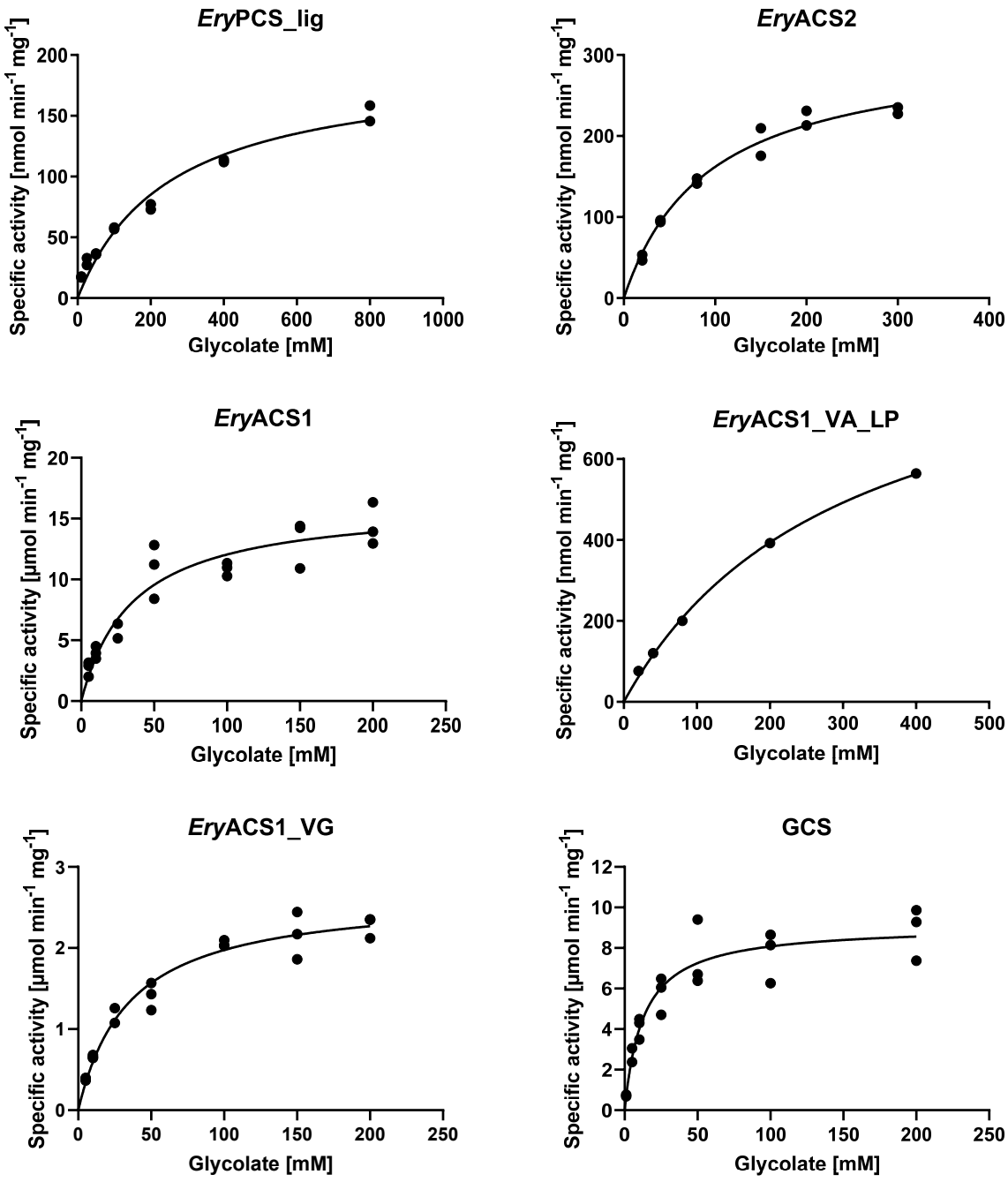

Supplementary Figure 22. Michaelis-Menten kinetics of different acyl-CoA synthetases. *Ery*PCS_lig: ligase domain of propionyl-CoA synthase from *Erythrobacter* sp. NAP1, *Ery*ACS2: acetyl-CoA synthetase 2 from *Erythrobacter* sp. NAP1, *Ery*ACS1: acetyl-CoA synthetase 1 from *Erythrobacter* sp. NAP1, *Ery*ACS1_VA_LP: acetyl-CoA synthetase 1 from *Erythrobacter* sp. NAP1 with two mutations (V379A and L641P), *Ery*ACS1_VG: acetyl-CoA synthetase 1 from *Erythrobacter* sp. NAP1 with V379G mutation, GCS: acetyl-CoA synthetase 1 from *Erythrobacter* sp. NAP1 with V379A mutation. Each data point for for n=3 independent measurements (EryACS1, EryACS1_VG, GCS), n=2 independent measurements (EryPCS_lig, EryACS2) or a single measurement (n=1, EryACS1_VA_LP) is shown. The data were analysed using nonlinear regression.

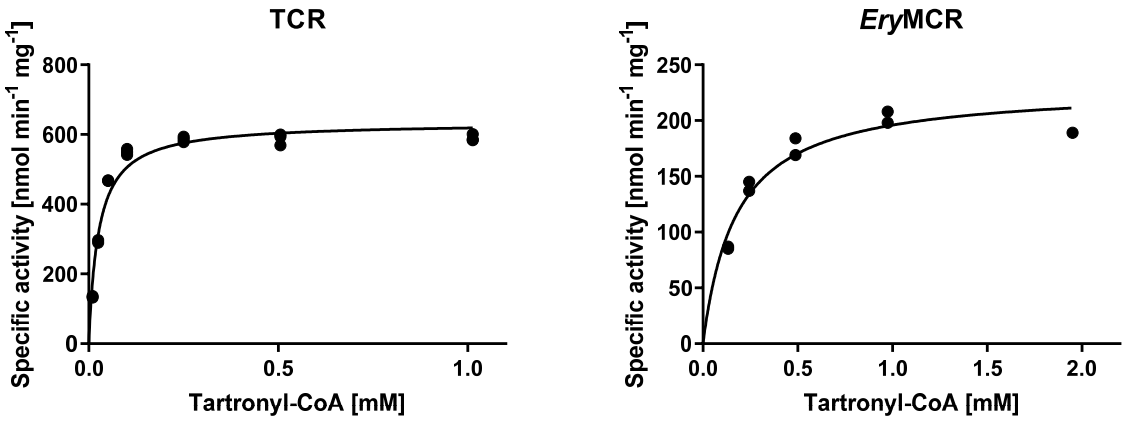

Supplementary Figure 23. Michaelis-Menten kinetics of tartronyl-CoA reduction by two tested isoenzymes of malonyl-CoA reductases. *Ca*MCR/TCR: malonyl-CoA reductase of *C. aurantiacus*. *Ery*MCR: malonyl-CoA reductase of *Erythrobacter sp*. NAP1. Each data point for n=3 (TCR) or n=2 independent measurements (EryMCR) is shown. The data were analysed using nonlinear regression.

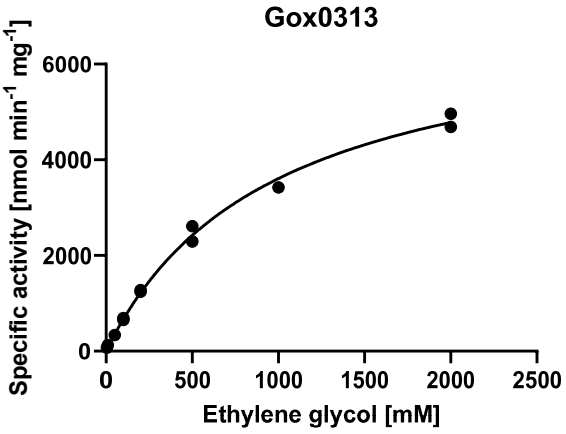

Supplementary Figure 24. Michaelis-Menten kinetics of alcohol dehydrogenase Gox0313 from *Gluconobacter oxydans*. Each data point for n=2 independent measurements is shown. The data were analysed using nonlinear regression.

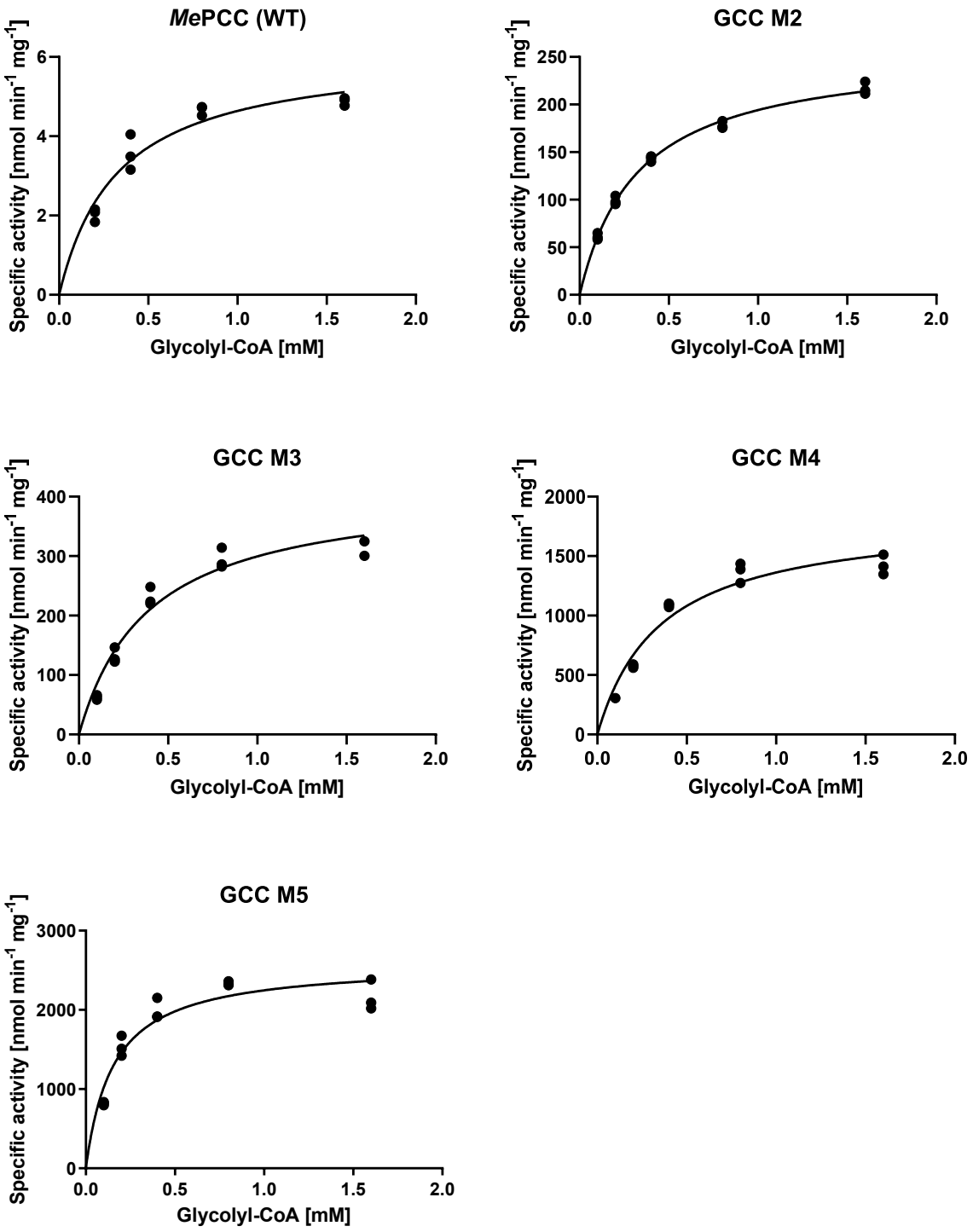

Supplementary Figure 25. Michaelis-Menten kinetics of glycolyl-CoA carboxylation. *Me*PCC (WT): propionyl-CoA carboxylase of *Methylorubrum extorquens* AM1, GCC M2: *Me*PCC with Y143H and D407I mutations, GCC M3: *Me*PCC with L100S, Y143H and D407I mutations, GCC M4: *Me*PCC with L100S, Y143H, D407I and I450V mutations, GCC M5: *Me*PCC with L100S, Y143H, D407I, I450V and W502R mutations. Each data point for n=3 independent measurements is shown. The data were analysed using nonlinear regression.

Supplementary Tables

Supplementary Table 1. Enzymes characterized in this study.

Reaction	Abbr.	mutation(s)	Full name	Organism	v_{max} [nmol min^{-1} mg^{-1}]	app. K_M [mM]	k_{cat}/K_M [M^{-1} s^{-1}]
glycolate → gCoA	*Cp*PCT	n/a	Propionate CoA transferase	*Clostridium propionicum*	32 ± 3	149 ± 35 (glycolate)	0.2
glycolate → gCoA	*Re*PCT	n/a	propionate CoA transferase	*Ralstonia eutropha*	1,300 ± 70	52 ± 10 (glycolate)	25
glycolate → gCoA	AbfT	n/a	4-OH-butyrate CoA transferase	*Clostridium aminobutyricum*	5,500 ± 1,500	34 ± 11 (glycolate)	129
glycolate → gCoA	*Ery*PCS_lig	n/a	ligase domain of pCoA synthase	*Erythrobacter* sp. NAP1	192 ± 14	252 ± 45 (glycolate)	1.3
glycolate → gCoA	*Ery*ACS2	n/a	acyl-CoA synthetase	*Erythrobacter* sp. NAP1	311 ± 16	92 ± 12 (glycolate)	4
glycolate → gCoA	*Ery*ACS1	n/a	acyl-CoA synthetase	*Erythrobacter* sp. NAP1	450 ± 10	30 ± 2 (glycolate)	20
glycolate → gCoA	*Ery*ACS1*	n/a	acyl-CoA synthetase	*Erythrobacter* sp. NAP1	16,320 ± 1116	35 ± 8 (glycolate)	567
glycolate → gCoA	*Ery*ACS1_VA_LP	V379A, L641P	acyl-CoA synthetase	*Erythrobacter* sp. NAP1	984 ± 54	300 ± 30 (glycolate)	4
glycolate → gCoA	***Ery*ACS1_VA*, GCS**	**V379A**	**acyl-CoA synthetase**	***Erythrobacter* sp. NAP1**	**9,111 ± 508**	**13 ± 3 (glycolate)**	**853**
glycolate → gCoA	*Ery*ACS1_VG*	V379G	acyl-CoA synthetase	*Erythrobacter* sp. NAP1	2,666 ± 111	35 ± 5 (glycolate)	89
glycolate → gCoA	*Ery*ACS1_VS*	V379S	acyl-CoA synthetase	*Erythrobacter* sp. NAP1	not detectable	n/a	n/a
gCoA → tCoA	*Ca*PCC1	n/a	propionyl-CoA carboxylase	*Chloroflexus aurantiacus*	not detectable	n/a	n/a
gCoA → tCoA	*Ca*PCC2	n/a	propionyl-CoA carboxylase	*Chloroflexus aurantiacus*	not detectable	n/a	n/a
gCoA → tCoA	*Ery*PCC	n/a	propionyl-CoA carboxylase	*Erythrobacter* sp. NAP1	not detectable	n/a	n/a
gCoA → tCoA	*Me*PCC‡	n/a	propionyl-CoA carboxylase	*Methylorubrum extorquens* AM1	6 ± 0.4	0.33 ± 0.06 (gCoA)	41
gCoA → tCoA	*Me*PCC_DI	D407I	propionyl-CoA carboxylase	*Methylorubrum extorquens* AM1	30†	n/a	n/a
gCoA → tCoA	*Me*PCC_DK	D407K	propionyl-CoA carboxylase	*Methylorubrum extorquens* AM1	instable complex	n/a	n/a
gCoA → tCoA	*Me*PCC_GA	G170A	propionyl-CoA carboxylase	*Methylorubrum extorquens* AM1	not detectable	n/a	n/a
gCoA → tCoA	*Me*PCC_GS	G170S	propionyl-CoA carboxylase	*Methylorubrum extorquens* AM1	not detectable	n/a	n/a
gCoA → tCoA	*Me*PCC_GT	G170T	propionyl-CoA carboxylase	*Methylorubrum extorquens* AM1	not detectable	n/a	n/a
gCoA → tCoA	*Me*PCC_LD	L140D	propionyl-CoA carboxylase	*Methylorubrum extorquens* AM1	not detectable	n/a	n/a
gCoA → tCoA	*Me*PCC_LN	L140N	propionyl-CoA carboxylase	*Methylorubrum extorquens* AM1	not detectable	n/a	n/a
gCoA → tCoA	*Me*PCC_YE	Y143E	propionyl-CoA carboxylase	*Methylorubrum extorquens* AM1	not detectable	n/a	n/a
gCoA → tCoA	*Me*PCC_YH	Y143H	propionyl-CoA carboxylase	*Methylorubrum extorquens* AM1	20	n/a	n/a
gCoA → tCoA	*Me*PCC_YQ	Y143Q	propionyl-CoA carboxylase	*Methylorubrum extorquens* AM1	not detectable	n/a	n/a
gCoA → tCoA	GCC M2‡	Y143H, D407I	glycolyl-CoA carboxylase	*Methylorubrum extorquens* AM1	257 ± 5	0.33 ± 0.02 (gCoA)	1,687
gCoA → tCoA	GCC_M2_LD	L100D, Y143H, D407I	glycolyl-CoA carboxylase	*Methylorubrum extorquens* AM1	not detectable	n/a	n/a
gCoA → tCoA	GCC_M2_LN	L100N, Y143H, D407I	glycolyl-CoA carboxylase	*Methylorubrum extorquens* AM1	41	n/a	n/a
gCoA → tCoA	GCC M3‡	L100S, Y143H, D407I	glycolyl-CoA carboxylase	*Methylorubrum extorquens* AM1	416 ± 28	0.39 ± 0.07 (gCoA)	2,310
gCoA → tCoA	GCC_M3_DA	L100S, Y143H, D171A, D407I	glycolyl-CoA carboxylase	*Methylorubrum extorquens* AM1	instable complex	n/a	n/a
gCoA → tCoA	GCC_M3_DV	L100S, Y143H, D171V, D407I	glycolyl-CoA carboxylase	*Methylorubrum extorquens* AM1	not detectable	n/a	n/a
gCoA → tCoA	**GCC M4‡**	**L100S, Y143H, D407I, I450V**	**glycolyl-CoA carboxylase**	***Methylorubrum extorquens* AM1**	**1,841 ± 117**	**0.35 ± 0.06 (gCoA)**	**11,387**
gCoA → tCoA	**GCC M5‡**	**L100S, Y143H, D407I, I450V, W502R**	**glycolyl-CoA carboxylase**	***Methylorubrum extorquens* AM1**	**2,590 ± 130**	**0.15 ± 0.03 (gCoA)**	**36,275**
tCoA → glycerate	***Ca*MCR, TCR**	**n/a**	**tartronyl-CoA reductase**	***Chloroflexus aurantiacus***	**635 ± 14**	**0.026 ± 0.003 (tCoA)**	**54,170**

Reaction	Abbr.	mutation(s)	Full name	Organism	v_{max} [nmol min^{-1} mg^{-1}]	app. K_M [mM]	k_{cat}/K_M [M^{-1} s^{-1}]
tCoA → glycerate	*Ery*MCR	n/a	tartronyl-CoA reductase	*Erythrobacter* sp. NAP1	230 ± 13	0.18 ± 0.04 (tCoA)	2,787
tCoA → TSA	*St*MCR	n/a	malonyl-CoA reductase	*Sulfolobus tokodaii*	140[1]	n/a	n/a
EG → GA	Gox0313	n/a	alcohol dehydrogenase	*Gluconobacter oxydans*	7086 ± 284	964 ± 84 (EG)	4.7

Michaelis-Menten kinetic plots of all characterized enzymes can be found in Supplementary Figures 21-25. Data for v_{max} and app. K_M represent mean ± SD determined from n≥6 independent measurements using nonlinear regression. Enzymes in bold represent the enzyme variants used in the final TaCo pathway. n/a not applicable. *expressed in *E. coli* BL21 AI Δ*patZ*. † measured PK/LDH coupled. ‡ coexpressed with *M. extorquens* biotin ligase birA. [1]measured at 1 mM tartronyl-CoA.
gCoA: glycolyl-CoA, TSA: tartronic semialdehyde, tCoA: tartronyl-CoA, EG: ethylene glycol, GA: glycolaldehyde

Supplementary Table 2. Data collection, refinement, and model statistics.

	***Me*PCC**	**GCC-M5**
Data collection		
Microscope	Glacios	Titan Krios G3
Camera	K2	K3 (CDS)
Magnification	36.000 x	105.000 x
Voltage (kV)	200	300
Electron exposure (e–/Å2)	50.2	55.0
Defocus range (μm)	0.5-3.5	0.5-2.7
Pixel size (Å)	1.18	0.851
Image processing		
Symmetry imposed	C1	C1
Initial particle images (no.)	168.488	5.398.283
Final particle images (no.)	77.714	2.181.317
Applied B-factor ($Å^2$)	-86.6	-71.7
Final resolution (Å)	3.48	1.96
Refinement Statistics		
Modeling software	COOT, Phenix	COOT, Phenix
Protein residues	4702	4289
Ligands	6× CoA, 6× biotin	6× CoA, 6× biotin
Water	-	871
Map CC (volume)	0.83	0.86
RMS deviations		
Bond lengths (Å)	0.008	0.007
Bond angles (°)	0.761	0.972
ADP (B-factors)		
min / max / mean		
Protein	50.92 / 184.73 / 99.60	3.64 / 71.26 / 24.93
Ligand	102.25 / 136.29 / 124.46	30.41 / 40.40 / 36.62
Water	-	5.86 / 29.25 / 11.77
Ramachandran plot (%)		
Outliers	0.00	0.00
Allowed	6.36	2.70
Favored	93.64	97.30
Rotamer outliers (%)	0.00	0.00
MolProbity score	1.85	1.11
Clash score	7.95	2.07
Resolution (Å) at FSC of 0.143		
masked / unmasked	3.44 / 3.48	1.94 / 1.95
PDB Accession	**6YBP**	**6YBQ**
EMDB Accession	**EMD-10770**	**EMD-10771**

Supplementary Table 3. Kinetic parameters of different glycolyl-CoA carboxylase variants.

	k_{cat} [s^{-1}]	app. K_M [mM]	k_{cat}/K_M [M^{-1} s^{-1}]	k_{cat} [s^{-1}]	app. K_M [mM]	k_{cat}/K_M [M^{-1} s^{-1}]
		glycolyl-CoA			propionyl-CoA	
WT	0.013 ± 0.001	0.33 ± 0.06	40.7	26.2 ± 1.9	0.24 ± 0.04	1.09×10^5
M2	0.56 ± 0.01	0.33 ± 0.02	1.71×10^3	0.1 ± 0.002	0.42 ± 0.03	2.36×10^2
M3	0.9 ± 0.1	0.39 ± 0.07	2.31×10^3	0.2 ± 0.01	0.44 ± 0.06	5.17×10^2
M4	4.0 ± 0.3	0.35 ± 0.06	1.13×10^4	1.1 ± 0.04	0.45 ± 0.05	2.49×10^3
M5	5.6 ± 0.3	0.15 ± 0.03	3.62×10^4	11.9 ± 0.4	0.18 ± 0.02	6.63×10^4

Data for k_{cat} and app. K_M represent mean ± SD determined from n=18 independent measurements using nonlinear regression.

Supplementary Table 4. Comparison of different natural and synthetic photorespiratory bypasses.

	NPR	GLC[19]	OX[20]	A5P[1]	3OHP[22]	TACO
CO_2 release	yes	yes	yes	no	no	no
Place of CO_2 release	mitochondria (far RuBisCO)	chloroplast (near RuBisCO)	chloroplast (near RuBisCO)	no CO_2 released	no CO_2 released	no CO_2 released
Carbon efficiency‡	75%	75%	0%	100%	150%	150%
Way of CO_2-re-fixation	complete CBB cycle	complete CBB cycle	complete CBB cycle	part of CBB cycle	Included in bypass	Included in bypass
NH_3 release	yes	no	no	no	no	no
no. of enzymes needed	11	5	6	5	12	5
Turns of Calvin cycle	**4.8**	**4.8**	**12**	**4**	**3**	**3**
No. of RuBisCO carboxylation (75%)/ oxygenation (25%)	**3.6/ 1.2**	**3.6/ 1.2**	**9/ 3**	**3/ 1**	**2.25/ 0.75**	**2.25/ 0.75**
ATP consumed	**14**	**13.4**	**32**	**12**	**11.75**	**11 / 13.8***
Redox power consumed	**8 NAD(P)H + 1.2 Fd_{red}**	**7.4 NAD(P)H**	**14 NAD(P)H**	**7 NAD(P)H**	**6.5 NAD(P)H**	**6.5 NAD(P)H**

The values in the last four rows (in bold) were calculated from flux balance analysis (FBA) and are based on the net fixation of three CO_2 and formation of one 3-PGA.

NPR: Natural (canonical) photorespiration, GLC: glycerate bypass, OX: glycolate oxidation pathway, A5P: arabinose-5-phosphate shunt, 3OHP: 3-hydroxypropionate bypass, TACO: tartronyl-CoA pathway

* The values include the unfruitful ATP hydrolysis of the GCC M5 variant.
‡ Carbon efficiency relates to one complete turn of each of the photorespiratory pathways. For the calculations, we assumed that natural (canonical) photorespiration, the glycerate bypass and the glycolate pathway start with 2 molecules of 2-phosphoglycolate (i.e. with two oxygenation events), while the arabinose-5-phosphate shunt, the 3-OH-propionate bypass and the tartronyl-CoA pathway start with 1 molecule of 2-phosphoglycolate (i.e. with one oxygenation event).

Supplementary Table 5. Comparison of energy and carbon efficiencies of the CETCH cycle coupled with the glycerate pathway or the TaCo pathway.

	CETCH (v5.4) [6] + glycerate pathway	**CETCH (v5.4) + TaCo**
CO_2 fixed (per 3-PGA)	4	3
CO_2 release (per 3-PGA)	1	0
Carbon efficiency	**75%**	**100%**
turns of CETCH required (per 3-PGA)	2	1
ATP consumed	3	5
Redox power consumed	9 NAD(P)H	7 NAD(P)H

The values correspond to the formation of 3-phosphoglycerate (3-PGA).

Supplementary Table 6. Primers used in this study

name	sequence (5' → 3')
ACS_E_L641P	CGGACCCGTCTCTGGTGGATCGTCCGATTGAGGGCCGTCAG
ACS_Ery_V379A	CTGCGTCTGCTGGGCTCTGTAGGTGAGCCGATCAAC
ACS_Ery_V379G	CCCTGCGTCTGCTGGGCTCTGGAGGTGAGCCGATCAAC
ACS_Ery_V379S	GTTCCCTGCGTCTGCTGGGCTCTTCAGGTGAGCCGATCAAC
BirA_Me_bb_for	TATAGAATTCAGATCTAGGAGATATACATATGCAGTTCCG
BirA_Me_bb_rev	TATACTCGAGGGATCCCTATCCAGTCTCAGGCCG
BirA_Me_EcoRI_mut	CTGCTCGAATTTCTGTCGGAAC
MC60	TGCACCATATGTCGAGTCCAAAGATCGG
MC61	CTGACGGTACCTGCGACTAGTTCATTTATGGGGAAGATTGGCAACG
patZ_KO_fw	GAACAGTTAGAAAGCGTTTAAAATCATTCGGTCACTTCTGCGGGAGACCGGTAATTAACCCTCACTAAAGGGCG
patZ_KO_rv	CAATAATAACACCAGTCCCGATTAAGTGGTCAACATTTCCAGTACCTTACTAATACGACTCACTATAGGGCTC
PCC_G170A	CGTGCGCGGGCGCCGACGTGTACTCGCCG
PCC_G170S	CGTGCGCGGGCAGCGACGTGTACTCGC
PCC_G170T	CGTGCGCGGGCACCGACGTGTACTCGC
PCC_L100D	GTTCGGCGGCTCGGACTCCGAGGCGCACGCAG
PCC_L100N	GTTCGGCGGCTCGAACTCCGAGGCGCACGCAG
PCC_L100S	GTTCGGCGGCTCGTCCTCCGAGGCGCACGCAG
PCC_Y143H	GCGCTCGGCGGCCACGGCGAGGTGTTCCGC
PccB_fw_P1	GTTTAACTTTAATAAGGAGATATACCATGGGCAGCAGCCATC
PccB_rv_P1	GATTACTTTCTGTTCGACTTAAGCATTATGCGGCCGCAAG
PCCMe_D171A	CGTGCGCGGGCGGCGCCGTGTACTCGC
PCCMe_D171V	CGTGCGCGGGCGGCGTCGTGTACTCGC
PCCtoACC_D407I	CAAGGCCTTCGGCGGCGCCTACATCGTCATGGCCTCCAAGCATG
PCCtoGCC_D407K	CAAGGCCTTCGGCGGCGCCTACAAAGTCATGGCCTCCAAGCATG
PCCtoGCC_L140D	GAGGGCGTGGCCGCGGACGGCGGCTACGGC
PCCtoGCC_L140N	GAGGGCGTGGCCGCGAACGGCGGCTACGGC
PCCtoGCC_Y143E	CGCGCTCGGCGGCGAAGGCGAGGTGTTCCGCCG
PCCtoGCC_Y143Q	CGCGCTCGGCGGCCAAGGCGAGGTGTTCCGCCG
pET16b_NcoI2NdeI	CTTTAAGAAGGAGATATACATATGGCCATCATCATCATC

Supplementary Table 7. List of plasmids for heterologous expression.

abbreviation	full name	source organism	mutation(s)	plasmid	GenBank accession no.	reference
AbfT	4-hydroxybutyrate CoA transferase	*Clostridium aminobutyricum*	n/a	pTE1138	CAB60036.2	this work
BirA	biotin ligase	*Methylorubrum extorquens* AM1	n/a	pJZ152	WP_003598178.1	this work
***Ca*MCR, TCR**	malonyl-CoA/ tartronyl-CoA reductase	*Chloroflexus aurantiacus*	n/a	pTrc–McrCa	WP_012258473.1	[9]
***Ca*PCC1**	propionyl-CoA carboxylase	*Chloroflexus aurantiacus*	n/a	pJZ95	YP_001636422.1, YP_001635958.1	this work
***Ca*PCC2**	methylcrotonyl-CoA carboxylase	*Chloroflexus aurantiacus*	n/a	pJZ96	YP_001634995.1, YP_001635635.1	this work
***Cp*PCT**	propionate CoA transferase	*Clostridium propionicum*	n/a	pET-16b_PCT	CAB77207.1	[26]
Eno	enolase	*Escherichia coli*	n/a	pCA24N-eno	APC52982.1	ASKA[7]
***Ery*ACS1**	acyl-CoA synthetase	*Erythrobacter sp.* NAP1	n/a	pTE1007	WP_007165025.1	this work
***Ery*ACS1_VA, GCS**	acyl-CoA synthetase	*Erythrobacter sp.* NAP1	V379A	pTE1417	n/a	this work
***Ery*ACS1_VA_LP**	acyl-CoA synthetase	*Erythrobacter sp.* NAP1	V379A, L641P	pTE1427	n/a	this work
***Ery*ACS1_VG**	acyl-CoA synthetase	*Erythrobacter sp.* NAP1	V379G	pTE1434	n/a	this work
***Ery*ACS1_VS**	acyl-CoA synthetase	*Erythrobacter sp.* NAP1	V379S	pTE1418	n/a	this work
***Ery*ACS2**	acyl-CoA synthetase	*Erythrobacter sp.* NAP1	n/a	pTE1008	WP_007166279.1	this work
***Ery*MCR**	malonyl-CoA/ tartronyl-CoA reductase	*Erythrobacter sp.* NAP1	n/a	pTE1010	WP_007163680.1	this work
***Ery*PCC**	propionyl-CoA carboxylase	*Erythrobacter sp.* NAP1	n/a	pJZ151	WP_007163953.1, WP_007163945.1	this work
***Ery*PCS_lig**	ligase domain of propionyl-CoA synthase	*Erythrobacter sp.* NAP1	n/a	pJZ26	WP_007163681.1	this work
FucO	lactaldehyde reductase	*Escherichia coli*	n/a	pCA24N-fucO	WP_000013588.1	ASKA[7]
GCC M2	glycolyl-CoA carboxylase	*Methylorubrum extorquens* AM1	Y143H, D407I	pJZ133	n/a	this work
GCC M3	glycolyl-CoA carboxylase	*Methylorubrum extorquens* AM1	L100S, Y143H, D407I	pTE1412	n/a	this work
GCC M4	glycolyl-CoA carboxylase	*Methylorubrum extorquens* AM1	L100S, Y143H, D407I, I450V	pTE3100	n/a	this work
GCC M4	glycolyl-CoA carboxylase	*Methylorubrum extorquens* AM1	L100S, Y143H, D407I, I450V	pTE3100	n/a	this work
GCC M5	glycolyl-CoA carboxylase	*Methylorubrum extorquens* AM1	L100S, Y143H, D407I, I450V, W502R	pTE3101	n/a	this work
GCC_M2_LD	glycolyl-CoA carboxylase	*Methylorubrum extorquens* AM1	L100D, Y143H, D407I	pTE1411	n/a	this work
GCC_M2_LN	glycolyl-CoA carboxylase	*Methylorubrum extorquens* AM1	L100N, Y143H, D407I	pTE1413	n/a	this work
GCC_M3_DA	glycolyl-CoA carboxylase	*Methylorubrum extorquens* AM1	L100S, Y143H, D171A, D407I	pTE1422	n/a	this work
GCC_M3_DV	glycolyl-CoA carboxylase	*Methylorubrum extorquens* AM1	L100S, Y143H, D171V, D407I	pTE1425	n/a	this work
GlxK	glycerate kinase	*Escherichia coli*	n/a	pCA24N-glxK	WP_062863124.1	ASKA[7]
Gox0313	alcohol dehydrogenase	*Gluconobacter oxydans*	n/a	pTE1453	AAW60096.1	this work
Gox1801	succinic semialdehyde reductase	*Gluconobacter oxydans*	n/a	pTE1125	WP_011253321.1	this work
Gpm	phosphoglycerate mutase	*Escherichia coli*	n/a	pCA24N-gpmI	APC53800.1	ASKA[7]
MatB	malonyl-CoA synthetase	*Rhizobium leguminosarum*	n/a	pEMatB-nHis	AAC83455.1	[27]
Myo	myokinase (adenylate kinase)	*Escherichia coli*	n/a	pCA24N-adk	WP_127790717.1	ASKA[7]
Nox	NADH Oxidase	*Lactobacillus pentosus*	n/a	pET28a-NH-nox-L.p.	WP_050338260.1	[28]

abbreviation	full name	source organism	mutation(s)	plasmid	GenBank accession no.	reference
PCC	propionyl-CoA carboxylase	*Methylorubrum extorquens* AM1	n/a	pTE615	WP_003599287.1, WP_003597263.1	[6]
PCC_DI	propionyl-CoA carboxylase	*Methylorubrum extorquens* AM1	D407I	pJZ105	n/a	this work
PCC_DK	propionyl-CoA carboxylase	*Methylorubrum extorquens* AM1	D407K	pJZ103	n/a	this work
PCC_GA	propionyl-CoA carboxylase	*Methylorubrum extorquens* AM1	G170A	pJZ127	n/a	this work
PCC_GS	propionyl-CoA carboxylase	*Methylorubrum extorquens* AM1	G170S	pJZ117	n/a	this work
PCC_GT	propionyl-CoA carboxylase	*Methylorubrum extorquens* AM1	G170T	pJZ118	n/a	this work
PCC_LD	propionyl-CoA carboxylase	*Methylorubrum extorquens* AM1	L140D	pJZ99	n/a	this work
PCC_LN	propionyl-CoA carboxylase	*Methylorubrum extorquens* AM1	L140N	pJZ100	n/a	this work
PCC_YE	propionyl-CoA carboxylase	*Methylorubrum extorquens* AM1	Y143E	pJZ101	n/a	this work
PCC_YH	propionyl-CoA carboxylase	*Methylorubrum extorquens* AM1	Y143H	pJZ141	n/a	this work
PCC_YQ	propionyl-CoA carboxylase	*Methylorubrum extorquens* AM1	Y143Q	pJZ102	n/a	this work
PduP	propionaldehyde dehydrogenase	*Rhodopseudomonas palustris* BisB18	n/a	pJZ73	WP_041801450.1	[29]
Pgp	2-PG phosphatase	*Escherichia coli*	n/a	pCA24N-gph	APC54031.1	ASKA[7]
PPK2-I	polyphosphate kinase	*Sinorhizobium meliloti*	n/a	pET28a-SmPPK2	n/a	[16]
PPK2-II	polyphosphate kinase	*Acinetobacter johnsonii*	n/a	pET28a-AjPPK2	n/a	[16]
***Re*PCT**	propionate CoA transferase	*Ralstonia eutropha*	n/a	pET-19b::pct	CAJ93797.1	[30]
***Cd*SucD**	succinyl-CoA reductase	*Clostridioides difficile*	n/a	pTE1816	WP_004454646	this work

n/a - not applicable, 2-PG: 2-phosphoglycolate

Supplementary Table 8. Conditions for heterologous expression in *E. coli* and purification of enzymes.

Enzyme abbr.	full name	tag	strain[1]	medium[2]	resistance[3]	induction	expression	purification
AbfT	4-hydroxybutyrate CoA transferase	His	Rosetta	GLB	Amp	0.5 mM IPTG	25 °C O/N	b
AKR7a2	succinic semialdehyde reductase	His	BL21	TB	Amp	0.25 mM IPTG	21°C O/N	e
***Ca*MCR, TCR**	malonyl-CoA/ tartronyl-CoA reductase	Strep	BL21	GLB	Amp	0.5 mM IPTG	25 °C 4h	c
***Ca*PCC1**	propionyl-CoA carboxylase	His	BL21 DE3	GLB	Amp	0.4 mM IPTG	37°C 4h	f
***Ca*PCC2**	propionyl-CoA carboxylase	His	BL21 DE3	GLB	Amp	0.4 mM IPTG	37°C 4h	f
Ccr	Crotonyl-CoA carboxylase/reductase	His	BL21	TB	Amp	0.25 mM IPTG	21°C O/N	e
***Cd*SucD**	succinyl-CoA reductase	His	Rosetta	GLB	Spec	0.5 mM IPTG	25 °C O/N	b, e
***Ck*SucD**	succinyl-CoA reductase	His	BL21	TB	Spec	0.25 mM IPTG	21 °C O/N	e
***Cp*PCT**	propionate CoA transferase	His	BL21	TB	Amp	0.5 mM IPTG	25 °C O/N	a
Ecm	ethylmalonyl-CoA mutase	His	BL21	TB	Amp	0.25 mM IPTG	21°C O/N	e
Epi	ethylmalonyl-CoA/ methylmalonyl-CoA epimerase	His	BL21	TB	Amp	0.25 mM IPTG	21°C O/N	e
***Ery*ACS, GCS**	acyl-CoA synthetase	His	AI	TB	Amp	0.5 mM IPTG	25 °C 4h	a
***Ery*ACS, GCS**	acyl-CoA synthetase	His	AI Δ*patZ*	TB	Amp + Kan	0.5 mM IPTG + 0.02% ara	25 °C 4h	a
***Ery*MCR**	malonyl-CoA/tartronyl-CoA reductase	Strep	BL21	TB	Amp	0.5 mM IPTG	25 °C O/N	c
***Ery*PCC**	propionyl-CoA carboxylase	His	BL21 DE3	GLB	Spec	not induced	25°C O/N	a
***Ery*PCS_lig**	ligase domain of propionyl-CoA synthase	His	BL21	TB	Amp	0.5 mM IPTG	25 °C O/N	a
Fdh	formate dehydrogenase (D221A)	His	BL21	TB	Amp	0.25 mM IPTG	21°C O/N	e
FucO	lactaldehyde reductase	His	BL21	TB	Cam	0.5 mM IPTG	25 °C O/N	a
GCC	glycolyl-CoA carboxylase	His	BL21_BirA	GLB[4]	Spec + Amp	0.5 mM IPTG	25 °C O/N	a
GlxK	glycerate kinase	His	BL21	TB	Cam	0.5 mM IPTG	25 °C O/N	a
Gox0313	alcohol dehydrogenase	His	BL21	TB	Amp	0.5 mM IPTG	25 °C O/N	a
Gox1801	succinic semialdehyde/ glyoxylate reductase	Strep	Rosetta	GLB	Amp	0.5 mM IPTG	25 °C O/N	d
Gpm	phosphoglycerate mutase	His	BL21	TB	Cam	0.5 mM IPTG	25 °C O/N	a
KatE	katalase	His	BL21	TB	Cam	0.25 mM IPTG	21°C O/N	e
Mch	mesaconyl-CoA hydratase	His	BL21	TB	Amp	0.25 mM IPTG	21°C O/N	e
Mcl1	β-methylmalyl-CoA lyase	His	BL21	TB	Amp	0.25 mM IPTG	21°C O/N	e
Mcm	methylmalonyl-CoA mutase	His	BL21	TB	Amp	0.25 mM IPTG	21°C O/N	e
Mco	methylsuccinyl-CoA oxidase	His	Rosetta	TB	Amp	0.25 mM IPTG	21°C O/N	e
***Me*PCC**	propionyl-CoA carboxylase	His	BL21_BirA	GLB[4]	Spec + Amp	0.5 mM IPTG	25 °C O/N	a
Myo	myokinase (adenylate kinase)	His	BL21	TB	Cam	0.5 mM IPTG	25 °C O/N	a
Nmar0206	4-hydroxybutyryl-CoA synthetase	His	BL21 GroES/GroEL	TB	Amp	0.25 mM IPTG	21°C O/N	e
Nmar0207	4-hydroxybutyryl-CoA dehydrogenase	His	BL21	TB[5]	Amp	0.25 mM IPTG	21°C O/N	e
Nox	NADH Oxidase	His	BL21	GLB	Kan	0.5 mM IPTG	25 °C O/N	a
Pco	propionyl-CoA oxidase	His	Rosetta	TB	Amp	0.25 mM IPTG	25°C 4h	e

Enyzme abbr.	full name	tag	strain[1]	medium[2]	resistance[3]	induction	expression	purification
PduP	propionaldehyde dehydrogenase	Strep	BL21	TB	Amp	not induced	25 °C O/N	c
Pgp	phosphoglycolate phosphatase	His	BL21	TB	Cam	0.5 mM IPTG	25 °C O/N	a
Ppk2-I	polyphosphate kinase	His	BL21	TB	Kan	0.25 mM IPTG	21°C O/N	e
Ppk2-II	polyphosphate kinase	His	BL21	TB	Kan	0.25 mM IPTG	21°C O/N	e
***Re*PCT**	propionate CoA transferase	His	BL21	TB	Amp	0.5 mM IPTG	25 °C O/N	a

[1] see text "Bacterial Strains" in Supplementary Materials and Methods for details
[2] TB: terrific broth (12 g L^{-1} tryptone, 24 g L^{-1} yeast extract, 0.4% glycerol, 17 mM KH_2PO_4, 72 mM K_2HPO_4), GLB: golden LB (LB medium with 0.4% glycerol, 17 mM KH_2PO_4, 72 mM K_2HPO_4)
[3] concentrations of antibiotics in medium: ampicillin (Amp) 100 µg mL^{-1}, kanamycin (Kan) 50 µg mL^{-1}, chloramphenicol (Cam) 34 µg mL^{-1}, spectinomycin (Spec) 50 µg mL^{-1}
[4] PCC/GCC medium contained 2 µg mL^{-1} biotin
[5] Nmar0207 medium additives: 100 µM Fe(II)SO_4, 100 µM Fe(III)citrate, 20 mM fumarate

Supplementary References

1. Trudeau, D. L. *et al.* Design and in vitro realization of carbon-conserving photorespiration. *Proc. Natl. Acad. Sci. USA* **115**, E11455-E11464 (2018).
2. Peter, D. M., Vögeli, B., Cortina, N. S. & Erb, T. J. A Chemo-Enzymatic Road Map to the Synthesis of CoA Esters. *Molecules* **21**, 517 (2016).
3. Sambrook, J. F. & Russell, D. W. *Molecular Cloning: A Laboratory Manual*. 3rd edn, (Cold Spring Harbor Laboratory Press, New York, 2001).
4. Shenoy, A. R. & Visweswariah, S. S. Site-directed mutagenesis using a single mutagenic oligonucleotide and DpnI digestion of template DNA. *Anal. Biochem.* **319**, 335-336 (2003).
5. Tabor, S. & Richardson, C. C. A bacteriophage T7 RNA polymerase/promoter system for controlled exclusive expression of specific genes. *Proc. Natl. Acad. Sci. USA* **82**, 1074-1078 (1985).
6. Schwander, T., Schada von Borzyskowski, L., Burgener, S., Cortina, N. S. & Erb, T. J. A synthetic pathway for the fixation of carbon dioxide *in vitro*. *Science* **354**, 900-904 (2016).
7. Kitagawa, M. *et al.* Complete set of ORF clones of *Escherichia coli* ASKA library (A Complete Set of *E. coli* K-12 ORF Archive): Unique Resources for Biological Research. *DNA Res.* **12**, 291-299 (2005).
8. Meyer, M., Schweiger, P. & Deppenmeier, U. Succinic semialdehyde reductase Gox1801 from *Gluconobacter oxydans* in comparison to other succinic semialdehyde-reducing enzymes. *Appl. Microbiol. Biotechnol.* **99**, 3929-3939 (2015).
9. Kroeger, J. K., Zarzycki, J. & Fuchs, G. A spectrophotometric assay for measuring acetyl–coenzyme A carboxylase. *Anal. Biochem.* **411**, 100-105 (2011).
10. Fairhead, M. & Howarth, M. Site-specific biotinylation of purified proteins using BirA. *Methods Mol. Biol.* **1266**, 171-184 (2015).
11. Beneyton, T., Coldren, F., Baret, J.-C., Griffiths, A. D. & Taly, V. CotA laccase: high-throughput manipulation and analysis of recombinant enzyme libraries expressed in *E. coli* using droplet-based microfluidics. *Analyst* **139**, 3314-3323 (2014).
12. Beneyton, T. *et al.* Out-of-equilibrium microcompartments for the bottom-up integration of metabolic functions. *Nat. Commun.* **9**, 2391 (2018).
13. Beneyton, T. *et al.* High-throughput screening of filamentous fungi using nanoliter-range droplet-based microfluidics. *Sci. Rep.* **6**, 27223 (2016).
14. Fischlechner, M. *et al.* Evolution of enzyme catalysts caged in biomimetic gel-shell beads. *Nat. Chem.* **6**, 791-796 (2014).
15. Han, J., Gagnon, S., Eckle, T. & Borchers, C. H. Metabolomic analysis of key central carbon metabolism carboxylic acids as their 3-nitrophenylhydrazones by UPLC/ESI-MS. *Electrophoresis* **34**, 2891-2900 (2013).
16. Mordhorst, S., Siegrist, J., Müller, M., Richter, M. & Andexer, J. N. Catalytic Alkylation Using a Cyclic S-Adenosylmethionine Regeneration System. *Angew. Chem. Int. Ed.* **56**, 4037-4041 (2017).
17. Tran, T. H. *et al.* Structure and function of a single-chain, multi-domain long-chain acyl-CoA carboxylase. *Nature* **518**, 120-124 (2015).
18. Guan, X., Diez, T., Prasad, T. K., Nikolau, B. J. & Wurtele, E. S. Geranoyl-CoA carboxylase: a novel biotin-containing enzyme in plants. *Arch. Biochem. Biophys.* **362**, 12-21 (1999).
19. Kebeish, R. *et al.* Chloroplastic photorespiratory bypass increases photosynthesis and biomass production in Arabidopsis thaliana. *Nat. Biotechnol.* **25**, 593-599 (2007).

20. Maier, A. *et al.* Transgenic Introduction of a Glycolate Oxidative Cycle into *A. thaliana* Chloroplasts Leads to Growth Improvement. *Front. Plant Sci.* **3** (2012).
21. South, P. F., Cavanagh, A. P., Liu, H. W. & Ort, D. R. Synthetic glycolate metabolism pathways stimulate crop growth and productivity in the field. *Science* **363** (2019).
22. Shih, P. M., Zarzycki, J., Niyogi, K. K. & Kerfeld, C. A. Introduction of a synthetic CO_2-fixing photorespiratory bypass into a cyanobacterium. *J. Biol. Chem.* **289**, 9493-9500 (2014).
23. Hansen, R. W. & Hayashi, J. A. Glycolate metabolism in *Escherichia coli*. *J. Bacteriol.* **83**, 679-687 (1962).
24. Krakow, G., Barkulis, S. S. & Hayashi, J. A. Glyoxylic acid carboligase: an enzyme present in glycolate-grown *Escherichia coli*. *J. Bacteriol.* **81**, 509 (1961).
25. Zelcbuch, L. *et al.* An *in vivo* metabolic approach for deciphering the product specificity of glycerate kinase proves that both *E. coli*'s glycerate kinases generate 2-phosphoglycerate. *PLoS ONE* **10**, e0122957 (2015).
26. Selmer, T., Willanzheimer, A. & Hetzel, M. Propionate CoA-transferase from *Clostridium propionicum*: Cloning of the gene and identification of glutamate 324 at the active site. *Eur. J. Biochem.* **269**, 372-380 (2002).
27. Vagstad, A. L., Bumpus, S. B., Belecki, K., Kelleher, N. L. & Townsend, C. A. Interrogation of global active site occupancy of a fungal iterative polyketide synthase reveals strategies for maintaining biosynthetic fidelity. *J. Am. Chem. Soc.* **134**, 6865-6877 (2012).
28. Nowak, C. *et al.* A water-forming NADH oxidase from *Lactobacillus pentosus* suitable for the regeneration of synthetic biomimetic cofactors. *Front. Microbiol.* **6**, 957 (2015).
29. Zarzycki, J., Sutter, M., Cortina, N. S., Erb, T. J. & Kerfeld, C. A. *In Vitro* Characterization and Concerted Function of Three Core Enzymes of a Glycyl Radical Enzyme - Associated Bacterial Microcompartment. *Sci. Rep.* **7**, 42757 (2017).
30. Lindenkamp, N., Schürmann, M. & Steinbüchel, A. A propionate CoA-transferase of *Ralstonia eutropha* H16 with broad substrate specificity catalyzing the CoA thioester formation of various carboxylic acids. *Appl. Microbiol. Biotechnol.* **97**, 7699-7709 (2013).